Title

Decoupling Bulk Mechanics and Mono- and Multivalent Ion Transport in Polymers Based on Metalâ��Ligand Coordination

Journal

Chemistry of Materials, 30(16)

ISSN

0897-4756 1520-5002

Authors

Schauser, Nicole S
Sanoja, Gabriel E
Bartels, Joshua M
et al.

Publication Date

2018-08-13

DOI

10.1021/acs.chemmater.8b02633

Peer reviewed

Decoupling Bulk Mechanics and Mono- and Multivalent Ion Transport in Polymers Based on Metal-Ligand Coordination

Nicole S. Schauser,[a,‡] Gabriel E. Sanoja,[b,†,‡] Joshua Bartels,[b] Sheetal K. Jain,[c] Jerry Hu,[a] Song-I Han,[c] Lynn M. Walker,[d] Matthew E. Helgeson,[b] Ram Seshadri,[a] Rachel A. Segalman[a,b,*]

[a]Materials Department and Materials Research Laboratory, [b]Department of Chemical Engineering, [c]Department of Chemistry and Biochemistry, University of California, Santa Barbara, California, 93106, United States

[d]Department of Chemical Engineering, Center for Complex Fluids Engineering, Carnegie Mellon University, Pittsburgh, Pennsylvania, 15213, United States

ABSTRACT: Decoupling bulk mechanics and ion conduction in conventional ion conducting polymers is challenging due to their mutual dependence on segmental chain dynamics. Polymers based on dynamic metal-ligand coordination are promising materials toward this aim. This work examines the effect of the nature and concentration of metal bis(trifluoromethylsulfonyl)imide (MTFSI) salts on the mechanical properties and ionic conductivity of poly[(ethylene oxide)-*stat*-(allyl glycidyl ether)] functionalized with tethered imidazole ligands (PIGE). Varying the cation identity of metal salts mixed in PIGE enables dramatic tunability of the zero-frequency viscosity from 0.3 kPa s to 100 kPa s. The ionic conductivity remains comparable at approximately 16 μS cm^{-1} among mono-, di- and trivalent salts at constant metal-to-ligand molar ratios due to negligible changes in glass transition temperatures at low ion concentrations. Thus, polymers based on metal-ligand coordination enable decoupling of polymer zero-frequency viscosity from ion conduction. Pulsed-field-gradient NMR on PIGE containing Li^+ or Zn^{2+} salts complement electrochemical impedance spectroscopy to demonstrate that both the anion and cation contribute to ionic conductivity.

Introduction

The outstanding mechanical properties of associating polymers have enabled novel functional materials for engineering,[1-2] biomedicine,[3-5] and energy storage.[6-7] Associating polymers can be formed from a variety of transient interactions including π-π stacking,[8] Diels-Alder adducts,[9] electrostatic forces,[10] hydrogen bonds,[1, 11-12] and metal-ligand (M-L) coordination.[13-15] M-L interactions are particularly interesting since they enable precise control of bulk properties through the nature and concentration of metal-ligand complexes with well-defined coordination geometry and large tunability in interaction timescale.[16-17] While the effect of M-L interactions on the mechanics of associating polymers has been well-studied,[18-24] the use of such systems as ion conducting polymers remains relatively unexplored. A recent investigation on these materials demonstrates that the zero-frequency viscosity and ionic conductivity are governed by processes with distinct relaxation times, suggesting that the transient nature of the M-L bonds plays a role in ion transport.[25]

The viscoelastic response of associating polymers is governed by the lifetime of the physical crosslinks. Above the percolation threshold, these materials behave as elastic rubbers at shorter times and flow as liquids otherwise.[26-28] The timescale of breakage and reformation of M-L coordination complexes depends on the nature and concentration of the metal and ligand, parameters that can be readily tuned without significant synthetic efforts.[13, 17] This flexibility results from a strategy in which the polymer is first synthesized, post-functionalized with a variety of ligands, and finally dynamically crosslinked with a transition metal salt. Seminal work on poly(4-vinylpyridine) based on Pd^{2+} or Pt^{2+} coordinated by *N,C,N*-pincer ligands illustrates that the linear mechanical response of polymers based on M-L interactions is universally described by the dissociation rate of model small-molecule coordination complexes.[13, 16] However, quantitative prediction of M-L polymer dynamic moduli using model small-molecule M-L complexes in solution remains limited, with discrepancies in behavior between the model compounds and their polymeric equivalents presumably arising as a result of chain connectivity, solvent concentration, and cooperativity.[20] Nevertheless, the bulk mechanical properties can be widely controlled based on the identity and concentration of metal and ligand, enabling the rational design of complex engineering materials.[29]

Polymer mechanics also plays an integral role in ion conduction due to the coupling between ion transport and local segmental dynamics.[30] Polymers containing solvating groups, such as ether oxygens in poly(ethylene oxide), facilitate salt dissociation by preferentially interacting with the cation while hindering its motion through the polymer matrix.[31-34] This issue is exacerbated for multivalent ions because of stronger interactions with solvating moieties that result in lower cation mobilities and ionic conductivities.[35-37] These ion-polymer interactions are at the core of the tradeoff between ion concentration and mobility

prompting the design of polymer electrolytes with low glass transition temperatures (T_g).[33, 38-40] However, low T_g polymers are not mechanically robust at the temperatures required to operate many energy conversion and storage devices motivating the development of novel molecular designs for high-performance materials.[41]

Previous work to decouple the bulk mechanical and ion conducting properties has focused on the use of either nanostructured materials (*e.g.*, block copolymers[42-43] and polymer nanocomposites[44-45]) or chemically crosslinked polymer networks.[46-47] Although numerous studies on nanostructured materials have illustrated the role of structure on ionic conductivity, their bulk performance ultimately depends on the long-range ion transport enabled by the percolation of the conducting domains. Chemically crosslinked polymer networks are often tedious to optimize because their properties are extremely sensitive to synthetic conditions. More importantly, these materials exhibit reductions in the ionic conductivity upon crosslinking due to an increase in T_g with concomitant detrimental effects on segmental dynamics and ion mobility.

This study illustrates the connection between the mechanics and ionic conductivity of a series of polymers based on M-L coordination composed of mono-, di-, and trivalent metal bis(trifluoromethylsulfonyl)imide salts (MTFSI) incorporated in a poly(ethylene oxide) with tethered imidazole groups. As expected from previous investigations on analogous materials, the dynamic moduli and terminal relaxation time are dependent on the identity of the metal species.[13, 16-17] However, in contrast to the dramatic tunability of the linear viscoelastic response, the ionic conductivity is relatively independent of salt identity. The ability to control the terminal relaxation time separately from local segmental motion at low ion concentration potentially enables the decoupling of the bulk mechanical and ion conducting properties within a specific concentration regime. Comparisons between ^{7}Li and ^{19}F pulsed-field-gradient NMR with electrochemical impedance spectroscopy in the polymer mixed with LiTFSI and $Zn(TFSI)_2$ reveal that the $TFSI^-$ anion is not the only species contributing to conductivity, suggesting that Li^+ and Zn^{2+} contribute to the ionic conductivity. While the ion-conducting polymers investigated here do not possess conductivities high enough for device application, the ability to decouple the polymer mechanical response from the ionic conductivity represents a promising route for future optimization.

Scheme 1. Synthesis of imidazole-functionalized PIGE copolymer and subsequent addition of metal salts allows for unique control of bulk properties. Various MTFSI salts (Li^+, Ni^{2+}, Cu^{2+}, Zn^{2+}, and Fe^{3+}) are added in controlled molar ratios of metal to imidazole ligand (*r*-ratios) to understand the role of M-L interactions and concentration on mechanical properties and ionic conductivity. The cations preferentially coordinate with the imidazole ligand, forming dynamic cross-links between polymer chains.

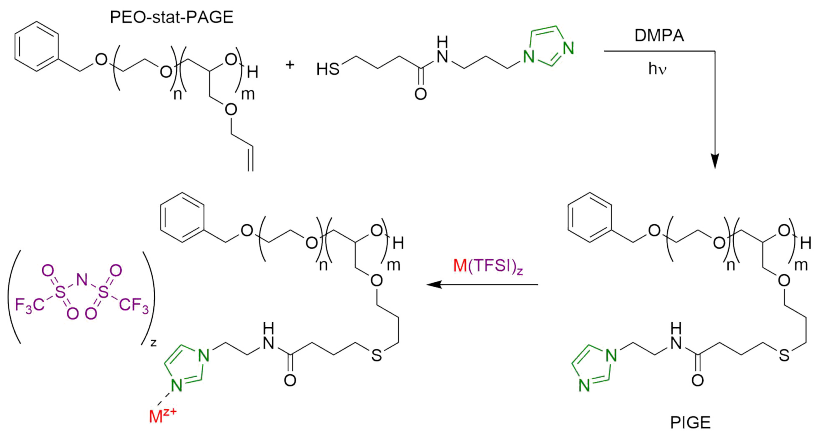

Experimental

Synthesis of imidazole-functionalized copolymer (PIGE)

The synthesis of the imidazole-functionalized poly[(ethylene oxide)-*stat*-(allyl glycidyl ether)] (PIGE) polymer used in this study was previously reported in Sanoja et al (Scheme 1) and is based on a combination of ionic copolymerization and click chemistry.[25] First, the allyl functionalized copolymer (PEO-stat-PAGE) was synthesized using epoxide ring opening anionic copolymerization of ethylene oxide (EO) and allyl glycidyl ether (AGE), followed by UV (365 nm) activated thiol-ene click chemistry of N-(2-(1H-Imidazol-1-yl)propyl)-4-mercaptobutanamide (Im-SH). The resulting polymer was dried *in vacuo* at 55 °C and immediately transferred to a nitrogen glove box to mitigate moisture uptake.

Synthesis of polymers PEO-stat-PAGE and PIGE containing metal salt

Samples of ion-conducting polymers were prepared in a nitrogen glove box by mixing stock solutions of polymer and anhydrous metal salts (0.1 M) in anhydrous methanol. The metal salts used for this study were LiTFSI, $Ni(TFSI)_2$ and $Fe(TFSI)_3$ (anhydrous, Alfa Aesar), and $Zn(TFSI)_2$ and $Cu(TFSI)_2$ (anhydrous, Alfa Aesar and Solvionic). Salts from two manufacturers were acquired for Zn^{2+} and Cu^{2+},

with subtle differences detected throughout the measurements. Unless explicitly stated, the measurements reported here are for salts sourced from Alfa Aesar. Controlled ratios of metal cation (M^{z+}) to imidazole (Im) ligand (r = [M^{z+}]:[Im]), for PIGE, or equivalently of metal cation to AGE (r = [M^{z+}]:[AGE]) for PEO-stat-PAGE polymers, of r = 0.05, r = 0.083 and r = 0.1 were prepared by stoichiometrically mixing appropriate amounts of the polymer and salt solutions. The resulting solutions were stirred in the glove box at 40 °C until they were homogenously mixed.

Molecular characterization

Size exclusion chromatography was performed on a Waters instrument using a refractive index detector and Agilent PL gel 5 μm MiniMIX-D column. THF at 35 °C was used as the mobile phase with a flow rate of 1.0 mL min^{-1}. Polydispersity index (Đ) was determined against PEO narrow standards (Agilent). ^{1}H NMR spectra were collected on a Bruker Avance DMX 500 MHz. The molecular weight of the precursor PEO-stat-PAGE copolymer was determined using ^{1}H NMR end-group analysis (Figure S1). This spectrum was collected in $CDCl_3$ at a polymer concentration of 60 mg mL^{-1} with 128 scans and a pulse delay time of 5 s.

General protocol for sample preparation

All polymer samples were handled in a nitrogen glove box prior to characterization. Samples were drop cast from solution onto substrates (Teflon, clean ITO-coated glass, or aluminum DSC pans), and dried *in vacuo* at 55 °C first for 8 h in a vacuum chamber in the glovebox (1×10^{-3} Torr) and then for 1 h in a high vacuum oven (4×10^{-8} Torr).

Thermal characterization

Polymer samples were drop cast from solution into standard aluminum pans and dried as detailed above. The samples were briefly exposed to air between the final vacuum step and the sealing of the DSC pans. The glass transition temperature (T_g) was measured with a Perkin Elmer DSC 8000 on second heating at 20 °C min^{-1} using the onset method.

Mechanical characterization

Samples with a molar ratio r = 0.1 were drop cast onto Teflon sheets, dried as described above, and transferred to a TA Instruments ARG2 rheometer operating under dry nitrogen flow. Samples were loaded onto a temperature-controlled platen and contacted with an 8 mm parallel top plate for measurement. Sample thicknesses were approximately 200 μm. Dynamic frequency sweeps were performed over a range of temperature, frequency, and strain amplitude of 5 °C to 70 °C, 100 rad s^{-1} to 0.1 rad s^{-1}, and 0.1% to 10%, respectively. Strain sweeps at 10 rad s^{-1} confirmed that measurements were performed in the linear viscoelastic regime (Figure S4). Time-temperature superposition (TTS) was performed using horizontal shift factors with a reference temperature of 20 °C. TTS was not performed for the PEO-stat-PAGE samples, except for the Ni(TFSI)$_2$ in PEO-stat-PAGE.

^{1}H-^{7}Li 2D heteronuclear correlation NMR

A PIGE sample mixed with LiTFSI at a molar ratio r = 0.083 was drop cast onto Teflon, dried as described above, and packed into a solid-state NMR Teflon 4 mm rotor insert. The insert was centrifuged to yield a uniform sample, and subsequently sealed into a 4mm rotor. 1D ^{1}H and 2D ^{1}H-^{7}Li heteronuclear correlation spectra were collected at a spinning frequency of 10 kHz at room temperature in a 11.7 T magnet. For the 2D experiment, 128 increments with 64 number of scans were used with an indirect dimension spectral width of 20 ppm for ^{1}H. A recycle delay of 3 s and cross polarization (CP) contact time of 1.6 ms were used.

Ionic conductivity characterization

Ionic conductivity was measured using electrochemical impedance spectroscopy on samples sandwiched between parallel ITO blocking electrodes. ITO electrodes on glass substrates were cleaned via subsequent sonications of 5 min with detergent, deionized water, acetone and isopropyl alcohol followed by a 5 min UV/ozone treatment. A 1/8" or 3/16" hole was punched into 150 μm double-sided Kapton tape to define the cell surface area. Samples with a molar ratio r = 0.05 and r = 0.1 were drop cast into the Kapton spacer placed on the ITO coated glass and dried as described above. Samples were sealed with a second ITO electrode under inert atmosphere, with sample thicknesses ranging from 150 μm to 200 μm. Transparent ITO coated glass substrates were used to ensure complete contact of the sample to the electrodes. Both the Alfa Aesar and Solvionic Zn^{2+} and Cu^{2+} salts were investigated. AC impedance measurements were performed using a Biologic SP-200 potentiostat in a nitrogen glove box. A sinusoidal 100 mV signal was applied over a frequency range of 1 MHz to 1 Hz at temperatures ranging from 30 °C to 90 °C. The data was converted into dielectric storage and loss, and the ionic conductivities determined from the real component of conductivity at the maximum in tan(δ).[48] This method is equivalent to determining the ionic conductivity from the low frequency intercept of the impedance with the real axis. At least two samples were measured for each composition.

Determination of lithium transference number

The PIGE and PEO-stat-PAGE LiTFSI ion-conducting polymers at a molar ratio r = 0.083 were further characterized *via* DC polarization of symmetric lithium foil – polymer – lithium foil coin cells assembled in an argon glove box. Samples were drop cast on Teflon, dried as described above, and transferred to a 1/8" diameter hole within a 50 μm thick Kapton spacer on top of lithium foil. Coin cells were assembled, transferred to an oven set to 80 °C, and equilibrated for up to 48 h until the interfacial resistance, monitored via electrochemical impedance spectroscopy (EIS), stabilized. This indicated the complete formation of a solid-electrolyte interphase (SEI) layer. Then, a 100 mV potential bias was applied and the resulting current measured as a function of time. EIS measurements were performed periodically to evaluate changes in the interfacial resistance. Lithium transference numbers were calculated following the method of Bruce and Vincent[49-50]

$$t_+ = \frac{I_{ss}(\Delta V - I_\Omega R_0)}{I_\Omega(\Delta V - I_{ss}R_{ss})} \quad (1)$$

Here, ΔV is the applied potential (100 mV), R_0 and R_{ss} are the initial and steady-state interfacial resistances, respectively, I_{ss} is the steady-state current, and I_Ω is the initial current determined from Ohm's Law

$$I_\Omega = \frac{\Delta V}{R_\Omega} \quad (2)$$

where R_Ω is the initial cell resistance (bulk and interfacial) measured by AC impedance. Using I_Ω instead of the initial current eliminates measurement errors related to the speed at which the instrument can record the initial current.[51]

Pulsed-field-gradient (PFG) NMR

Samples at a molar ratio r = 0.083 were drop cast onto Teflon and dried as described above. In a nitrogen glovebox, the polymers were packed with a spatula into thick-walled glass capillaries and centrifuged to yield uniform 4 cm-long samples. The capillaries were centered in medium-walled NMR tubes and sealed with high-pressure caps before measurement.

PFG NMR measurements were performed on a Bruker Avance III super widebore spectrometer equipped with a Bruker DIFF50 diffusion probe tuned to ^{7}Li and ^{19}F nuclei with replaceable radio frequency (RF) inserts. ^{19}F diffusion measurements of the TFSI$^-$ anion were performed on the Li^+ and Zn^{2+} PEO-stat-PAGE and PIGE samples at temperatures ranging from 30 °C to 80 °C. Diffusion measurements were not possible for the Ni^{2+}, Cu^{2+}, or Fe^{3+}-containing samples due to line broadening by the paramagnetic relaxation effects. ^{7}Li diffusion measurements were performed between 30 °C and 75 °C on the Li^+ PEO-stat-PAGE sample and at 80 °C on the Li^+ PIGE sample. Lower temperatures for the Li^+ PIGE could not be explored due to the low cation diffusion coefficient. Samples were equilibrated at each temperature for 15 min before measurement. A pulse sequence of stimulated echoes with bipolar pulses was used to measure diffusion coefficients. The attenuation of the echo (E) was fit to

$$E = exp\left[-\gamma^2 g^2 \delta^2 D(\Delta - \frac{\delta}{3})\right] \quad (3)$$

where γ is the gyromagnetic ratio, g is the gradient strength, δ is the gradient pulse length, Δ is the interval between gradient pulses (diffusion time), and D is the diffusion coefficient. The intervals between gradient pulses used for the acquisitions ranged from 20 ms to 40 ms for ^{7}Li and from 15 ms to 20 ms for ^{19}F. The pulse lengths used for acquisitions ranged from 4 ms to 5 ms for ^{7}Li and 1 ms to 4 ms for ^{19}F. For each diffusion measurement, 16 experiments of varying gradient strength up to a maximum of 2300 G cm^{-1} were performed. All measured attenuations were adequately fit with single exponential decays. Two samples were measured for the PIGE polymers, while only one was measured for the PEO-stat-PAGE samples.

The PFG NMR experiments were analyzed in the context of dilute solution theory. Within this framework, an ionic conductivity can be calculated from the measured diffusion coefficients using the Nernst-Einstein equation[52]

$$\sigma = \frac{F^2}{RT}(z_+^2 c_+ D_+ + z_-^2 c_- D_-) \quad (4)$$

where F is Faraday's constant, R is the ideal gas constant, T is the absolute temperature, and $z_{+/-}$, $c_{+/-}$, and $D_{+/-}$ are the valency, concentration, and diffusion coefficient of the cation/anion respectively. PFG NMR probes ion diffusion on a characteristic lengthscale $\sqrt{D\Delta}$ on the order of 1 μm to 10 μm. While the characteristic lengthscale probed by impedance spectroscopy depends on more complex factors, it is generally assumed to be roughly equivalent to that of PFG NMR. Thus, a comparison of the conductivity extracted from each technique is reasonable, within the context of dilute solution theory. This theory neglects intermolecular interactions and assumes that the ionic species are completely dissociated.[52] Consequently, there might be discrepancies between the calculated and experimentally determined ionic conductivities, which could be due to either the diffusion coefficients measured *via* PFG NMR having contributions from a number of associated or aggregated species (inaccurate $D_{+/-}$ measurements), or incomplete salt dissociation (inaccurate estimation of $c_{+/-}$).[53-55] In the binary electrolytes investigated in this study, the anion TFSI$^-$ concentration will equal z_+c_+ under the assumption of full salt dissociation. Thus Equation 4 reduces to

$$\sigma = \frac{F^2 c_+}{RT}(z_+^2 D_+ + z_+ D_-) \quad (5)$$

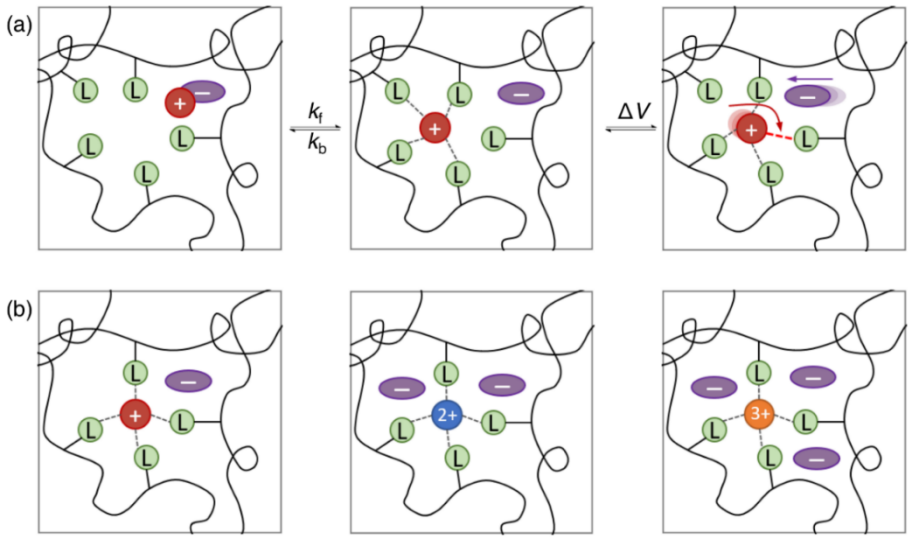

Figure 1. (a) Addition of metal salt to a polymer with tethered ligands results in an equilibrium between M-L coordination and salt dissociation. The application of an electric field allows for both ions to move, although the motion of coordinated cations is related to the timescale of metal-ligand coordination. (b) Addition of equal cation:ligand molar ratios (*r*) results in varying amounts of anions. In all figures, a fourfold coordination geometry is used for illustrative purposes.

Results and Discussion

To elucidate the effect of the nature and concentration of M-L bonds on the mechanical and ion conducting properties of polymers with tethered ligands, an array of mono- (Li^+), di- (Ni^{2+}, Zn^{2+}, Cu^{2+}), and trivalent (Fe^{3+}) MTFSI salts were incorporated into model PIGE at the controlled molar ratios of metal cations to pendant imidazoles (*r*-ratios). These neutral, nitrogen-linked, and pendant imidazoles (see Scheme 1) lack mobile protons that might contribute to the ionic conductivity, while enabling M-L interactions between the metal cations and the non-aromatic lone pair of the nitrogen in the imidazole ring. Note that due to the stoichiometry of salt dissociation, there is an increase in the concentration of anions with metal valency at constant *r*-ratios (Figure 1b). Moreover, the fraction of cations coordinated by imidazole and part of a M-L cross-link will depend on the preferred complex geometry and is expected to range between 4 and 6.[17] The weak electrostatic interactions resulting from large and charge-delocalized $TFSI^-$ anions resemble that of ionic liquids, yielding 'plasticized' and amorphous polymers which even at high ion concentrations exhibit low T_gs. A PEO backbone was investigated because its relatively high dielectric constant potentially enables sufficient salt dissociation and hinders ion aggregation to enhance ionic conductivity. Although the extent of dissociation results from a balance between the salt lattice energy, ion solvation, and M-L coordination (Figure 1a), the latter is expected to be the primary interaction dictating the bulk polymer properties as the equilibrium constant for metal cation-imidazole complexation is significantly larger than that of metal cation-crown ether solvation.[22,56-57] In the case of LiTFSI salt in PIGE, this is substantiated by ^{1}H-^{7}Li 2D NMR heteronuclear correlation, which reveals the proximity of Li^+ to imidazole ligands (Figure 2). The peak intensities of the imidazole protons (6.1-8.2 ppm) relative to the aliphatic protons on the PEO backbone (0-5.8 ppm) is significantly higher in the heteronuclear correlation (HETCOR) spectrum of ^{1}H coupled to ^{7}Li compared to direct 1D ^{1}H spectrum, as illustrated in Figure 2. In the 1D ^{1}H spectrum the ratio of the peak integrals of 6.1-8.2 ppm to 0-5.8 ppm peaks is ~0.13 which increases to ~1.32 in the HETCOR spectrum. This implies that the aliphatic protons are weakly coupled to the Li^+ whereas the imidazole protons have a relatively strong interaction to the Li^+ due to spatial proximity. The other cation species are expected to follow similar behavior.

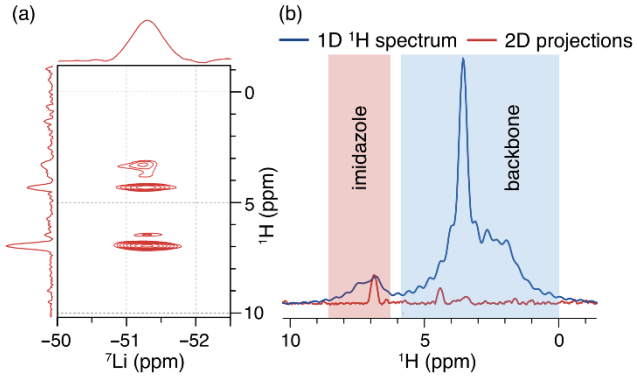

Figure 2. Solid-state NMR spectra demonstrate that cations interact preferentially with imidazole ligands. (a) 2D HETCOR ^{1}H-^{7}Li spectrum. (b) Comparison of 1D ^{1}H spectrum (red) with the projections of ^{1}H dimension (blue) from the 2D spectrum. This highlights the relative intensity changes of the ^{1}H peaks.

The dynamic nature of these M-L coordination bonds also allows for bond breakage and reformation on time scales that facilitate long-range cation transport. This mechanism of ion conduction is fundamentally different from that of anions as these weakly interact with polymers and have motion primarily dependent on the local segmental dynamics. Cation conduction through these systems would be maximum with extremely labile M-L coordination bonds. This physical picture is similar to that of conventional polymer electrolytes (PEO) which are composed

of nucleophilic polymer backbones that only solvate cations. The model PIGE is a statistical copolymer PEO_{323}-*stat*-$PIGE_{79}$ (M_n = 40 kDa, Đ < 1.2) with a constant mole fraction of imidazole moieties (x_{IGE} = 0.17) and was previously synthesized by Sanoja et. al.[25] DSC traces (Figure S3) demonstrate its amorphous nature, a result consistent with the suppression of PEO crystallization in an atactic backbone. The molecular properties and thermal transitions of the various polymers are summarized in Table 1.

Table 1. Properties of ion-conducting polymers.

Polymer	r^a	*wt%* salt	$T_g{}^b$ (°C)	σ (μS/cm) at 70 °C	σ (μS/cm) at $T - T_g$ = 90 °C
PIGE	0.0	0	–33	1.0 ±0.49	0.47 ±0.21
PIGE Li^+	0.1	4.8	–32	17 ±0.37	8.1 ±0.35
PIGE Ni^{2+}	0.1	9.8	–29	15 ±1.2	9.3 ±0.92
PIGE Cu^{2+} (AA)	0.1	9.9	–31	20 ±1.8	10 ±0.73
PIGE Cu^{2+} (S)	0.1	9.9	–25	13.6±1.6	10 ±1.1
PIGE Zn^{2+} (AA)	0.1	9.9	–28	20 ±0.7	13 ±0.33
PIGE Zn^{2+} (S)	0.1	9.9	–25	18 ±1.4	13 ±1.1
PIGE Fe^{3+}	0.1	13.6	–28	12 ±1.1	7.6 ±0.70

All polymers are based on the same PIGE precursor synthesized in Sanoja et. al.,[25] with a degree of polymerization of EO of 323 and of AGE of 79. [a] r = [M^{z+}:Imidazole].[b] Determined via differential scanning calorimetry. (AA)Salt acquired from Alfa Aesar. (S)Salt acquired from Solvionic.

I. Linear Polymer Mechanics

M-L coordination dramatically changes the bulk mechanical properties, as evidenced by a shift in the linear viscoelastic response to higher modulus and lower frequency upon incorporation of various MTFSI salts into PIGE (Figures 3a and 3b). These materials mechanically respond as dynamic networks with a plateau in the storage modulus at high frequencies, a crossover of the storage (G') and loss modulus (G''), and terminal relaxation similar to that of liquids.[26-28] The neat PIGE polymer is expected to be weakly entangled based on the molecular weight of the PEO backbone, with small contributions to elasticity relative to M-L cross-linking.[58] At an r-ratio of 0.1, the rheological signature of polymers with Ni^{2+} and Fe^{3+} clearly show a plateau in G' and a peak in G'' while that of polymers with Li^+, Cu^{2+}, and Zn^{2+} only reveal a slight increase in G' and decrease in terminal relaxation time indicating slower polymer dynamics. Although it is known that both Cu^{2+} and Zn^{2+} interact with imidazole to form dynamic crosslinks,[17, 29] there is an almost inconsequential change in the mechanical response that presumably results from either a change in cross-link concentration compared to the Ni^{2+} system, or the similarity in time-scale of M-L dissociation compared to relaxation of the entangled polymer melt. Additionally, all but the PIGE with Ni^{2+} and Fe^{3+} show liquid-like behavior at low frequency as evidenced by the scaling of $G' \sim \omega^2$ and $G'' \sim \omega$. The system based on Ni^{2+} yields the most dramatic change in the viscoelastic properties. Existing theories relate the modulus and terminal relaxation time scale with M-L ("sticker") binding kinetics.[26-27] M-L dissociation kinetics trends for the equivalent small-molecule M-L system in aqueous solution do not match the experimental trend of characteristic relaxation time in this study (see Supporting Information). As mentioned earlier, such discrepancies are perhaps expected since kinetic trends of M-L dissociation in aqueous solution neglect solvent cooperativity and polymer chain connectivity.[20] Further work is needed to determine the kinetics of M-L dissociation in polymer melts.

The effect of the MTFSI salts on the mechanical properties can be illustrated more clearly by inspecting the complex viscosity $|\eta^*| = \sqrt{(\eta')^2 + (i\eta'')^2}$, a property which describes the resistance of a fluid to undergo shear flow. More specifically, examination of its low frequency plateau η_0 (zero-frequency complex viscosity) is more convenient as this accounts for changes in crosslink concentration, polymer structure, and relaxation times with dynamic M-L bonds.[18, 28] Figure 3c illustrates an increase in η_0 upon addition of MTFSI to PIGE for all metal cations except for Li^+. The rheological similarity between PIGE and PIGE mixed with LiTFSI suggests that either each Li^+ interacts with only one imidazole thus not forming temporary crosslinks, or the timescale for interaction between Li^+ and imidazole is short compared to polymer dynamics. Interestingly, the increase over three orders of magnitude in η_0 does not correlate with T_g (Table 1), as the polymer with Ni^{2+} is significantly more viscous than that with Cu^{2+} or Zn^{2+} even though they all have $T_g \sim -30$ °C. This observation serves to demonstrate that the segmental dynamics, as expressed by T_g, and bulk polymer dynamics, as described by η_0, are decoupled, as the latter depends on the lability of M-L crosslinks. As will be discussed shortly, this is the fundamental reason that enables independent control over the mechanical and ion conducting properties through the identity of the metal cation.

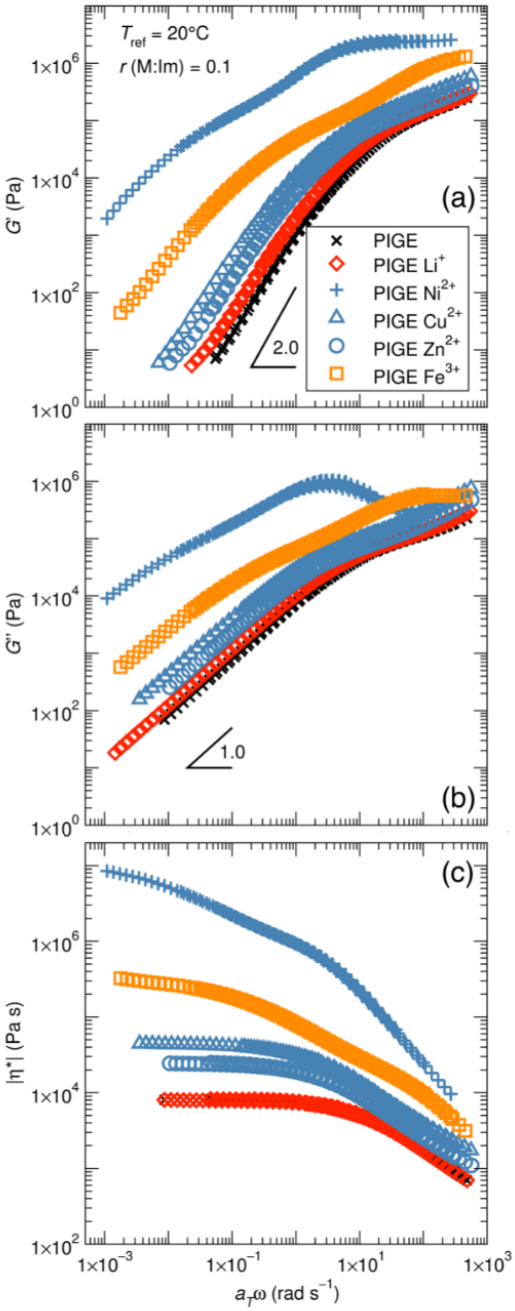

Figure 3. Mechanical properties of the polymer change drastically upon the addition of various metal salts. For the PIGE polymer containing covalently tethered ligands, Ni^{2+} and Fe^{3+} cations act as transient cross-linkers resulting in the appearance of a plateau in the storage modulus (a) and peak in the loss modulus (b) within the accessible frequency-temperature range. (c) A clearer effect of metal cross-linking can be seen from the complex viscosity, which increases dramatically with the addition of metal salts except for LiTFSI. Time-temperature superposition was successfully performed on all samples.

II. Ion Transport

The ionic conductivity of the PIGE-MTFSI is roughly independent of the identity of the metal cation (Figure 4, Tables 1 and 2). Its Vogel-Fulcher-Tamman (VFT) temperature-dependence reveals the importance of entropy and free volume on ion motion. As previously noted, there is a minimal shift in T_g across the polymer series that indicates that local segmental dynamics are not greatly affected by cation valency, identity, or anion concentration. This is, once again, why this material design enables independent tunability over bulk mechanical and ion conducting properties.

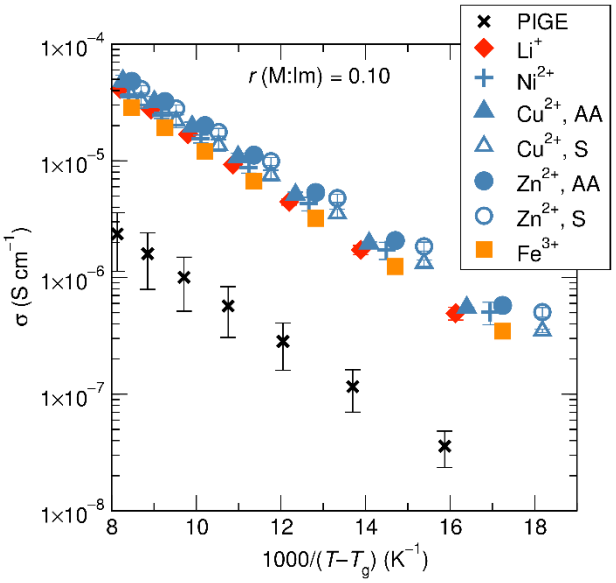

Figure 4. The ionic conductivity can be approximately normalized by the ratio of the concentration of metal to imidazole (r), regardless of ion valency or identity. Each data point results from an average of at least two different samples; error bars represent 68% confidence intervals.

Table 2. Ratios of the ionic conductivity of PIGE with di- and trivalent MTFSI salts to that of the same polymer containing monovalent LiTFSI.

$T - T_g$	$\frac{1000}{T-T_g}$	$\frac{\sigma_{Ni}}{\sigma_{Li}}$	$\frac{\sigma_{Zn}^{AA}}{\sigma_{Li}}$	$\frac{\sigma_{Zn}^{S}}{\sigma_{Li}}$	$\frac{\sigma_{Cu}^{AA}}{\sigma_{Li}}$	$\frac{\sigma_{Cu}^{S}}{\sigma_{Li}}$	$\frac{\sigma_{Fe}}{\sigma_{Li}}$
111.1	9	1.0	1.4	1.6	1.2	1.3	0.8
83.3	12	1.2	1.6	1.8	1.3	1.3	1.0
66.7	15	1.4	1.9	1.9	1.3	1.4	1.2

At three different reduced temperatures T-T_g the ratios are very close to 1 indicating that the ionic conductivity does not scale with ion valency as predicted by dilute solution theory. Divalent salts were acquired from [AA]Alfa Aesar and [S]Solvionic.

The decoupling of the polymer zero-frequency viscosity from ionic conductivity upon the inclusion of metal salts provides a promising route to stiffening polymers without compromising ion transport. From a fundamental standpoint, this is a consequence of the molecular processes governing ion transport and bulk mechanics. While the former primarily depends on the local segmental dynamics as quantified by T_g, the latter results from polymer self-diffusion through a sequence of M-L association and dissociation steps. At T = 70 °C, σ of PIGE-MTFSI is approximately 16 μS.cm^{-1} with no observable trend with the identity of the metal ion, while η_0 increases from 0.3 kPa.s to 100 kPa.s between Li^+ and Ni^{2+} (Figure 5). Again, the dramatic increase in η_0 is due to physical cross-linking and

changes in the lifetime of M-L coordination. These observations complement our previous investigation on the effect of ion concentration on the bulk properties of polymers based on M-L coordination[25] and allow us to develop rational design rules for high-performance materials. In particular, there is an optimum ionic conductivity due to the competing effects of increasing ion concentration and decreasing ion mobility,[25] with further stiffening enabled by changing the identity of the metal cation without detrimental effects to the ionic conductivity.

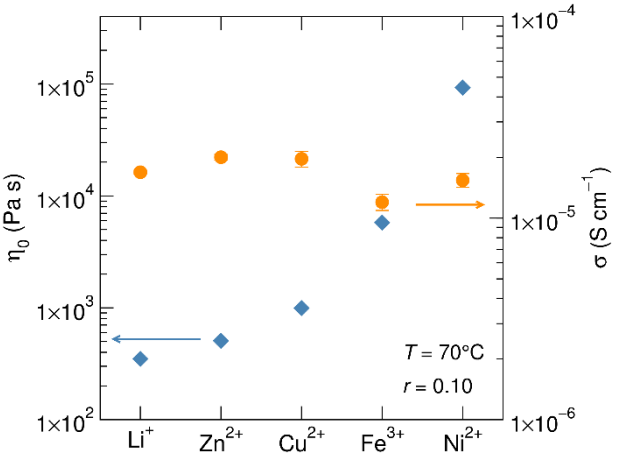

Figure 5. Polymers based on M-L coordination enable independent control over the mechanical and ion conducting properties. The zero-frequency viscosity of the material can be tuned over almost three orders of magnitude with minimal changes in the ionic conductivity. Error bars represent 68% confidence intervals.

Examination of the ionic conductivity within the framework of dilute solution theory not only demonstrates a complex tradeoff between ion mobility, valency, and ion concentration on ion transport but also serves to further investigate the fundamental reason why the ionic conductivity is coupled to segmental dynamics. Normalization of the ionic conductivity by the *r*-ratio yields a universal curve, a scaling behavior that is inconsistent with Equation 5, and vexing because the anion and overall ion concentration increase with metal valency. Assuming (1) full salt dissociation (strong electrolyte) and (2) that all metal cations have the same diffusion coefficient, it follows from Equation 5 that the contributions to the ionic conductivity from the cation and anion should scale with z_+^2 and z_+, respectively.[52] These are presumably invalid assumptions, yet they serve as a starting point to explain ion transport in polymers based on M-L coordination. If the contribution to the ionic current would be predominantly from the $TFSI^-$, a common feature in polymer electrolytes such as PEO/LiTFSI, the polymers with di- and trivalent salts would have a 2- or 3-fold increase in the ionic conductivity relative to their monovalent counterpart. Table 2 summarizes the ratio of the ionic conductivity of PIGE with di- and trivalent MTFSI salts to that of the same polymer containing monovalent LiTFSI. This ratio is evaluated at three different reduced temperatures (T-T_g) to account for differences in segmental dynamics among the polymers investigated, though this correction is inconsequential due to the negligible change in T_g with the identity of the MTFSI salts. Only at the lowest reduced temperature (T-T_g = 66.67 K), the PIGE based on Zn^{2+} is approximately twice as conductive as that based on Li^+, but for all other temperatures and metal cations the theoretical scaling does not hold. Similar results are observed for an *r*-ratio of 0.05 (Figure S8 and Tables S1-S3). This motivates a thorough reassessment of the comparison between measured ionic conductivity and predictions from dilute solution theory, and suggests that changes in diffusion coefficient or incomplete salt dissociation likely dominate the behavior of the M-L polymers studied here.

III. Ion Diffusion Coefficients and Dilute Solution Theory

The deviation from dilute solution theory of the ionic conductivity suggests a change in either the ion mobility or extent of dissociation with metal identity. Pulsed-field-gradient (PFG) NMR provides a powerful tool to investigate the role of ion mobility on conduction by probing the self-diffusion coefficients of NMR-active nuclei on a micrometer lengthscale.[53-54, 59] This technique does not distinguish between ions and aggregates composed of an NMR-active species unless their diffusion coefficients or chemical shifts are distinguishable over the experimental timescale (*i.e.*, in the absence of fast exchange between ion and aggregate states). Previous investigations on PEO-LiTFSI have demonstrated that the ion diffusion coefficients decrease with ion concentration,[54] an observation attributed to an increase in either polymer viscosity due to solvation or ion drag force from ion-ion interactions. If local chain dynamics are critical in the ion mobility of PIGE-MTFSI, a VFT normalization of the diffusion coefficient by T_g should yield a universal master curve irrespective of metal identity. This is indeed the case when examining the diffusion coefficient of $TFSI^-$ in PIGE with Li^+ and Zn^{2+} (Figure 6). The only subtle differences in diffusion coefficient not only implies that the metal identity as well as the anion concentration are only relevant insofar as they affect the polymer segmental dynamics, but also that these salts probably do not form significant aggregation, as changes in polymer viscosity are enough to account for the difference in diffusion coefficient of the salts. A similar comparison between the diffusion coefficient of $TFSI^-$ in PEO-stat-PAGE with Li^+ and Zn^{2+} does not yield the same universal scaling after normalizing for T_g (Figure S9). As will be discussed later, this is presumably due to incomplete dissociation of the MTFSI salts within the PEO-stat-PAGE, causing ion-ion interactions to affect the anion diffusion coefficient. Thus, we hypothesize that metal-imidazole coordination in the Li^+ and Zn^{2+} PIGE effectively screens the electrostatic interactions such that the cation identity and anion concentration do not play a key role on anion mobility.

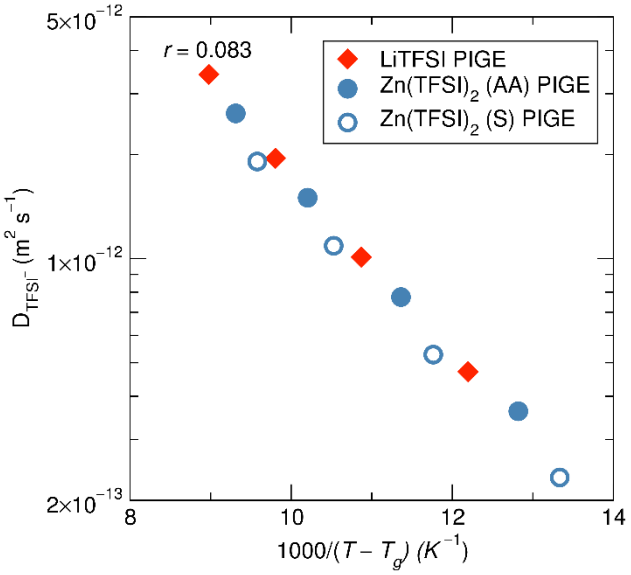

Figure 6. ^{19}F diffusion measurements reveal the nature of the cation and concentration of the anion do not play a role in the anion diffusivity in polymers based on M-L coordination. Although PIGE with Zn^{2+} has twice as much $TFSI^-$, the anion is just as mobile as in PIGE with Li^+ after accounting for differences in T_g.. (AA) and (S) refer to salt sourced from Alfa Aesar and Solvionic, respectively.

The anion diffuses faster than the cation in polymers based on M-L coordination, consistent with previous investigations on PEO-LiTFSI and presumably due to interactions of the cation with the polyether backbone or imidazole ligands.[33] ^{7}Li PFG NMR experiments on PIGE (Figure S10) enable measurement of the Li^+ diffusion coefficient and further calculation of the transference number within the context of dilute solution theory

$$t_+ = \frac{z_+ D_+}{z_+ D_+ + D_-} \quad (6)$$

where z_+ is the valency of the cation, and $D_{+/-}$ are the diffusion coefficients of the cation and anion. This analysis reveals that the Li^+ transference number in PIGE (0.19, at 80 °C) is slightly higher than that of the corresponding PEO-stat-PAGE system (0.15, at 75 °C). While this small difference could be attributed to temperature effects, the higher transference number in PIGE could also result from weaker Li^+-polymer interactions in the presence of imidazole. Whereas the Li^+ in the PEO-stat-PAGE polymer are solvated by ether oxygens and thus tightly wrapped by the polymer backbone, the Li^+ in the PIGE interact primarily with the imidazole, as demonstrated with ^{1}H-^{7}Li 2D heteronuclear correlation in Figure 2. This likely facilitates hopping between adjacent sites in the PIGE. These results are further supported by comparisons of the transference number with that determined via conventional chronoamperometry (Equation 1) in symmetric lithium foil – polymer electrolyte – lithium foil coin cells (0.18 at 80 °C).[49] The agreement demonstrates that the diffusion coefficients measured by PFG NMR do not have an important contribution from ion aggregates.

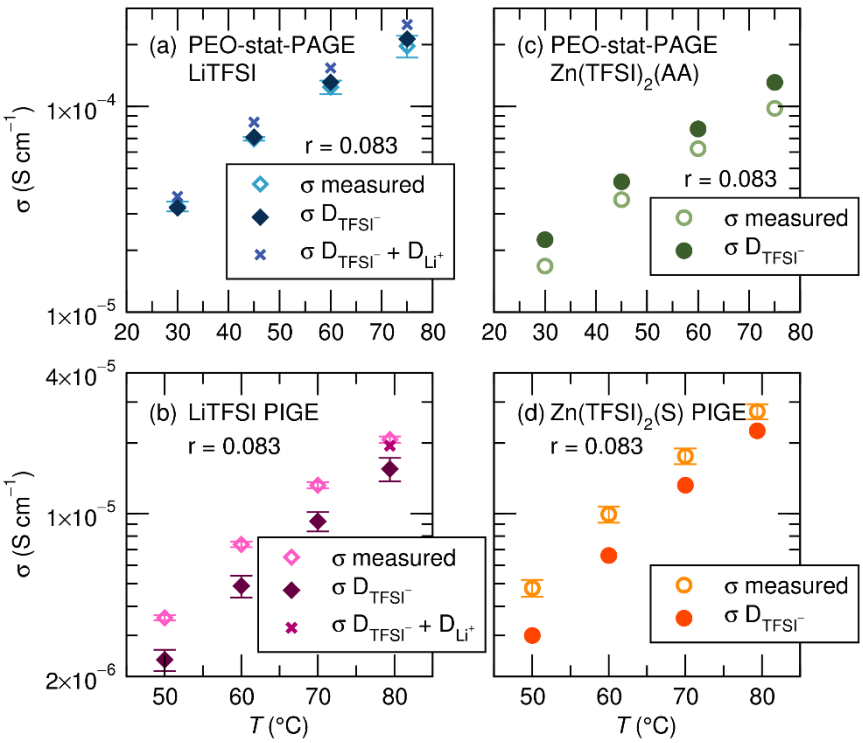

Figure 7. The comparison of measured conductivity values with calculated conductivity suggest incomplete salt dissociation for the PEO-stat-PAGE, and cation contribution to the conductivity for the PIGE. Conductivity is calculated using diffusion coefficients measured from pulsed-field-gradient NMR using the Nernst-Einstein equation assuming full salt dissociation. First only anion ($TFSI^-$) participation in ion conductivity is accounted for, and then for the lithium-containing polymers full participation from both Li^+ and $TFSI^-$ is assumed. In the PEO-stat-PAGE samples (a, c), an overestimation of conductivity compared to the measured conductivity

indicates incomplete salt dissociation, while in the PIGE samples (b, d) $TFSI^-$ diffusion underestimates the observed conductivity. Lithium diffusion adequately accounts for the remaining difference in LiTFSI PIGE (b), suggesting the possibility that zinc might account for the remaining difference in the $Zn(TFSI)_2$ PIGE (d). $Zn(TFSI)_2$ from Alfa Aesar was used for the PEO-stat-PAGE measurement, while the Solvionic salt was used for the PIGE measurement.

Comparison of the ionic conductivity with predictions from dilute solution theory indicate that the Li^+ and Zn^{2+} are mobile in PIGE (Figure 7). In PEO-stat-PAGE with Li^+, the ionic conductivity calculated with Equation 5 over-estimates that experimentally determined with AC impedance, especially when accounting for contributions from both ions. This observation indirectly suggests incomplete dissociation or aggregation of LiTFSI in PEO-stat-PAGE. A similar analysis on PIGE with Li^+ reveals that contributions of both the Li^+ and $TFSI^-$ are required to adequately capture the experimentally measured conductivity. The addition of the imidazole ligands presumably enhances salt dissociation such that the Nernst-Einstein relation in Equation 5 adequately describes the ionic conductivity. This comparison between theory and experiment becomes useful when analyzing the ionic conductivity and diffusivities of polymers based on Zn^{2+}.

In particular, incomplete dissociation is even more apparent in the PEO-stat-PAGE for $Zn(TFSI)_2$ than for LiTFSI. Though a Zn^{2+} diffusion coefficient cannot be measured with NMR, the ionic conductivity estimated with Equation 5 assuming single-ion $TFSI^-$ conductor ($D_+ = 0$) already overestimates the measured conductivity value. The Zn^{2+} PIGE system, however, underestimates the conductivity when only taking $TFSI^-$ diffusion into account (Figure 7 for Solvionic salt, and Figure S11 for Alfa Aesar salt). This suggests either the presence of an additional mobile ion, or that the $TFSI^-$ diffusion coefficient measured via PFG NMR does not adequately capture the true behavior of the ion. A combination of XRF, ^1H and ^{19}F NMR, and Karl Fischer (KF) titration corroborated the high purity (>99%) of the $Zn(TFSI)_2$ salt, indicating that the residual conductivity is likely due to mobile Zn^{2+} within the sample. Assuming all Zn^{2+} are dissociated and mobile, one can estimate with Equation 5 the diffusion coefficient that would be required to obtain the experimentally measured conductivity value. This analysis provides a lower bound of a diffusion coefficient of Zn^{2+} in PIGE of around 3×10^{-9} cm^2 s^{-1} at 80 °C, which would correspond to a transference number of 0.13 (see Supporting Information). Although the Zn^{2+} diffusion coefficient is about 35% that of Li^+, its higher valency provides leeway for an equivalent contribution to the ionic conductivity at slower ion motion.

Conclusion

The introduction of metal salts into a polymer matrix containing covalently tethered imidazole ligands enables the decoupling of mechanical properties from ionic conductivity. Polymers based on M-L coordination exhibit higher zero-frequency viscosities compared to the neat entangled polymer melt, with high sensitivity towards the identity of the metal cation due to the formation of dynamic M-L crosslinks. In contrast, the ionic conductivity of these materials is relatively insensitive to the metal cation identity and seems instead to be a function of cation to ligand ratio. Ion mobility in polymers is dictated to a significant extent by the local segmental dynamics, which remain largely unchanged with metal cation identity but depend more strongly on salt concentration. These results enable orders-of-magnitude changes in polymer zero-frequency viscosity with negligible changes in ionic conductivity. PFG NMR diffusion measurements performed on polymers based on Li^+ and Zn^{2+} demonstrate that $TFSI^-$ diffusion is insensitive to cation identity or anion concentration and only depends on polymer T_g. Interestingly this result only holds for the imidazole-containing polymer and not the PEO-stat-PAGE precursor. Whether this is a function of the extent of dissociation of the metal salt or is due to the nature of the M-L interaction with pendant imidazole groups merits further analysis. Lastly, diffusion measurements can be used to estimate an ionic conductivity assuming full salt dissociation. While it is known that impedance spectroscopy and PFG probe different timescales, this analysis for the PIGE with Zn^{2+} suggests that in addition to the $TFSI^-$, Zn^{2+} ions contribute to the ionic conductivity measured by electrochemical impedance spectroscopy. While Zn^{2+} ions appear to have lower diffusion coefficients than Li^+, their higher valence ensures that their contribution to the overall conductivity is significant, even comparable to what is seen in the case of Li^+ in PIGE. This work paves the way for future studies on polymers based on M-L coordination, suggesting multivalent systems can be designed with beneficial mechanical properties and no detriment to total ionic conductivity compared with monovalent salt species.

ASSOCIATED CONTENT

Supporting Information. The following files are available free of charge: ^1H NMR, GPC, DSC traces, strain sweeps for PIGE with M(TFSI), discussion on the connection between M-L dissociation kinetics and the zero-frequency viscosity, PFG NMR, calculation of the diffusion coefficient and transference number of Zn^{2+} in PIGE, rheology of PEO-*stat*-PAGE with M(TFSI), and other information.

AUTHOR INFORMATION

Corresponding Author

* R.A.S (segalman@ucsb.edu)

Present Addresses

† Sciences et Ingénierie de la Matière Molle, CNRS UMR 7615, École Supérieure de Physique et de Chimie Industrielles de la Ville de Paris (ESPCI), ParisTech, PSL Research University, 10 Rue Vauquelin, F-75231, Paris Cedex 05, France.

Author Contributions

‡These authors contributed equally.

Funding Sources

This work was supported by the MRSEC Program of the National Science Foundation under Award No. DMR 1720256 (IRG-2). N.S.S gratefully acknowledges the Fannie and John Hertz Foundation, the Holbrook Foundation Fellowship through the UCSB Institute for Energy Efficiency, and the National Science Foundation Graduate Research Fellowship Program under Grant No. 1650114. Any opinions, findings, and conclusions or recommendations expressed in this material

are those of the authors and do not necessarily reflect the views of the National Science Foundation. PIGE was synthesized by G.E.S. with funding from the Institute for Collaborative Biotechnologies through grant W911NF-09-0001 from the U.S. Army Research Office. The content of the information does not necessarily reflect the position or the policy of the Government, and no official endorsement should be inferred.

ACKNOWLEDGMENT

The authors would also like to thank Prof. Christopher Evans for initial conceptualization of the idea of ion transport in metal-ligand polymers

References

1. Cordier, P.; Tournilhac, F.; Soulié-Ziakovic, C.; Leibler, L. Self-Healing and Thermoreversible Rubber from Supramolecular Assembly. *Nature* **2008,** *451*, 977-980.
2. Enke, M.; Döhler, D.; Bode, S.; Binder, W. H.; Hager, M. D.; Schubert, U. S. Intrinsic Self-Healing Polymers Based on Supramolecular Interactions: State of the Art and Future Directions. In *Self-healing Materials*, Hager, M. D.; van der Zwaag, S.; Schubert, U. S. Eds. Springer International Publishing: Cham, 2016; 59-112.
3. Webber, M. J.; Appel, E. A.; Meijer, E. W.; Langer, R. Supramolecular Biomaterials. *Nat Mater* **2015,** *15*, 13-26.
4. Rosales, A. M.; Anseth, K. S. The Design of Reversible Hydrogels to Capture Extracellular Matrix Dynamics. *Nat Rev Mater* **2016,** *1*, 15012.
5. Chaudhuri, O.; Gu, L.; Klumpers, D.; Darnell, M.; Bencherif, S. A.; Weaver, J. C.; Huebsch, N.; Lee, H.-p.; Lippens, E.; Duda, G. N.; Mooney, D. J. Hydrogels with Tunable Stress Relaxation Regulate Stem Cell Fate and Activity. *Nat Mater* **2015,** *15*, 326-334.
6. Wang, C.; Wu, H.; Chen, Z.; McDowell, M. T.; Cui, Y.; Bao, Z. Self-Healing Chemistry Enables the Stable Operation of Silicon Microparticle Anodes for High-Energy Lithium-Ion Batteries. *Nat Chem* **2013,** *5*, 1042-1048.
7. Chen, D.; Wang, D.; Yang, Y.; Huang, Q.; Zhu, S.; Zheng, Z. Self-Healing Materials for Next-Generation Energy Harvesting and Storage Devices. *Adv Energy Mater* **2017,** *7*, 1700890.
8. Burattini, S.; Greenland, B. W.; Merino, D. H.; Weng, W.; Seppala, J.; Colquhoun, H. M.; Hayes, W.; Mackay, M. E.; Hamley, I. W.; Rowan, S. J. A Healable Supramolecular Polymer Blend Based on Aromatic π-π Stacking and Hydrogen-Bonding Interactions. *J Amer Chem Soc* **2010,** *132*, 12051-12058.
9. Sheridan, R. J.; Bowman, C. N. A Simple Relationship Relating Linear Viscoelastic Properties and Chemical Structure in a Model Diels–Alder Polymer Network. *Macromolecules* **2012,** *45*, 7634-7641.
10. Hunt, J. N.; Feldman, K. E.; Lynd, N. A.; Deek, J.; Campos, L. M.; Spruell, J. M.; Hernandez, B. M.; Kramer, E. J.; Hawker, C. J. Tunable, High Modulus Hydrogels Driven by Ionic Coacervation. *Adv Maters* **2011,** *23*, 2327-2331.
11. Sijbesma, R. P.; Beijer, F. H.; Brunsveld, L.; Folmer, B. J. B.; Hirschberg, J. H. K. K.; Lnage, R. F. M.; Lowe, J., K. L.; Meijer, E. W. Reversible Polymers Formed from Self-Complementary Monomers Using Quadruple Hydrogen Bonding. *Science* **1997,** *278*, 1601-1604.
12. Feldman, K. E.; Kade, M. J.; Meijer, E. W.; Hawker, C. J.; Kramer, E. J. Model Transient Networks from Strongly Hydrogen-Bonded Polymers. *Macromolecules* **2009,** *42*, 9072-9081.
13. Yount, W. C.; Loveless, D. M.; Craig, S. L. Strong Means Slow: Dynamic Contributions to the Bulk Mechanical Properties of Supramolecular Networks. *Angew Chem Int Ed* **2005,** *44*, 2746-2748.
14. Holten-Andersen, N.; Harrington, M. J.; Birkedal, H.; Lee, B. P.; Messersmith, P. B.; Lee, K. Y.; Waite, J. H. pH-Induced Metal-Ligand Cross-links Inspired by Mussel Yield Self-Healing Polymer Networks with Near-Covalent Elastic Moduli. *Proc Natl Acad Sci* **2011,** *108*, 2651-2655.
15. Mozhdehi, D.; Ayala, S.; Cromwell, O. R.; Guan, Z. Self-Healing Multiphase Polymers via Dynamic Metal–Ligand Interactions. *J Amer Chem Soc* **2014,** *136*, 16128-16131.
16. Yount, W. C.; Loveless, D. M.; Craig, S. L. Small-Molecule Dynamics and Mechanisms Underlying the Macroscopic Mechanical Properties of Coordinatively Cross-Linked Polymer Networks. *J Amer Chem Soc* **2005,** *127*, 14488-14496.
17. Mozhdehi, D.; Neal, J. A.; Grindy, S. C.; Cordeau, Y.; Ayala, S.; Holten-Andersen, N.; Guan, Z. Tuning Dynamic Mechanical Response in Metallopolymer Networks through Simultaneous Control of Structural and Temporal Properties of the Networks. *Macromolecules* **2016,** *49*, 6310-6321.
18. Xu, D.; Craig, S. L. Scaling Laws in Supramolecular Polymer Networks. *Macromolecules* **2011,** *44*, 5465-5472.
19. Grindy, S. C.; Lenz, M.; Holten-Andersen, N. Engineering Elasticity and Relaxation Time in Metal-Coordinate Cross-Linked Hydrogels. *Macromolecules* **2016,** *49*, 8306-8312.
20. Tang, S.; Olsen, B. D. Relaxation Processes in Supramolecular Metallogels Based on Histidine–Nickel Coordination Bonds. *Macromolecules* **2016,** *49*, 9163-9175.
21. Fullenkamp, D. E.; He, L.; Barrett, D. G.; Burghardt, W. R.; Messersmith, P. B. Mussel-Inspired Histidine-Based Transient Network Metal Coordination Hydrogels. *Macromolecules* **2013,** *46*, 1167-1174.
22. Rossow, T.; Habicht, A.; Seiffert, S. Relaxation and Dynamics in Transient Polymer Model Networks. *Macromolecules* **2014,** *47*, 6473-6482.
23. Groote, R.; Szyja, B. M.; Pidko, E. A.; Hensen, E. J. M.; Sijbesma, R. P. Unfolding and Mechanochemical Scission of Supramolecular Polymers Containing a Metal-Ligand Coordination Bond. *Macromolecules* **2011,** *44*, 9187-9195.
24. Filippidi, E.; Cristiani, T. R.; Eisenbach, C. D.; Waite, J. H.; Israelachivili, J. N.; Ahn, B. K.; Valentine, M. T. Toughening Elastomers using Mussel-Inspired Iron-Catechol Complexes. *Science* **2017,** *358*, 502-505.
25. Sanoja, G. E.; Schauser, N. S.; Bartels, J. M.; Evans, C. M.; Helgeson, M. E.; Seshadri, R.; Segalman, R. A. Ion Transport in Dynamic Polymer Networks Based on Metal-Ligand Coordination: Effect of Crosslinker Concentration. *Macromolecules* **2018,** *51*, 2017-2026.
26. Leibler, L.; Rubinstein, J. M.; Colby, R. H., Dynamics of Reversible Networks. *Macromolecules* **1991,** *24*, 4701-4707.
27. Tanaka, F.; Edwards, S. F. Viscoelastic Properties of Physically Crosslinked Networks. 1. Transient Network Theory. *Macromolecules* **1992,** *25*, 1516-1523.
28. Rubinstein, M.; Semenov, A. N. Dynamics of Entangled Solutions of Associating Polymers. *Macromolecules* **2001,** *34*, 1058-1068.
29. Grindy, S. C.; Learsch, R.; Mozhdehi, D.; Cheng, J.; Barrett, D. G.; Guan, Z.; Messersmith, P. B.; Holten-Andersen, N. Control of Hierarchical Polymer Mechanics with Bioinspired Metal-Coordination Dynamics. *Nat Mater* **2015,** *14*, 1210-1216.
30. Miller, T. F.; Wang, Z. G.; Coates, G. W.; Balsara, N. P. Designing Polymer Electrolytes for Safe and High Capacity Rechargeable Lithium Batteries. *Acc Chem Res* **2017,** *50*, 590-593.
31. Fenton, D. E.; Parker, J. M.; Wright, P. V. Complexes of Alkali Metal Ions with Poly(ethylene oxide). *Polymer* **1973,** *14*, 589.
32. Wheatle, B. K.; Keith, J. R.; Mogurampelly, S.; Lynd, N. A.; Ganesan, V. Influence of Dielectric Constant on Ionic Transport in Polyether- Based Electrolytes. *ACS Macro Lett* **2017,** *6*, 1362-1367.
33. Webb, M. A.; Jung, Y.; Pesko, D. M.; Savoie, B. M.; Yamamoto, U.; Coates, G. W.; Balsara, N. P.; Wang, Z.-G.; Miller, T. F. Systematic Computational and Experimental Investigation of Lithium-Ion Transport Mechanisms in Polyester-Based Polymer Electrolytes. *ACS Cent Sci* **2015,** *1*, 198-205.
34. Bruce, P. G.; Vincent, C. A. Polymer Electrolytes. *J Chem Soc Faraday Trans* **1993,** *89*, 3187-3203.
35. Farrington, G. C.; Linford, R. G. Poly(ethylene oxide) Electrolytes Containing Divalent Cations. In *Polymer Electrolyte Reviews II*, MacCallum, J. R.; Vincent, C. A., Eds. Elsevier: London, 1989; pp 255-284.

36. Lewandowski, A.; Stępniak, I.; Grzybkowski, W. Copper Transport Properties in Polymer Electrolytes Based on Poly(ethylene oxide) and Poly(acrylonitrile). *Solid State Ion* **2001,** *143*, 425-432.

37. Thelen, J. L.; Inceoglu, S.; Venkatesan, N. R.; Mackay, N. G.; Balsara, N. P. Relationship between Ion Dissociation, Melt Morphology, and Electrochemical Performance of Lithium and Magnesium Single-Ion Conducting Block Copolymers. *Macromolecules* **2016,** *49*, 9139-9147.

38. Shi, J.; Vincent, C. A. The Effect of Molecular Weight on Cation Mobility in Polymer Electrolytes. *Solid State Ion* **1993,** *60*, 11-17.

39. Borodin, O.; Smith, G. D. Mechanism of Ion Transport in Amorphous Poly(ethylene oxide)/LiTFSI from Molecular Dynamics Simulations. *Macromolecules* **2006,** *39*, 1620-1629.

40. Donoso, J. P.; Bonagamba, T. J.; Panepucci, H. C.; Oliveira, L. N.; Gorecki, W.; Berthier, C.; Armand, M. Nuclear Magnetic Relaxation Study of Poly(ethylene oxide)–Lithium Salt Based Electrolytes. *J Chem Phys* **1993,** *98*, 10026-10036.

41. Monroe, C.; Newman, J. The Impact of Elastic Deformation on Deposition Kinetics at Lithium/Polymer Interfaces. *J Electrochem Soc* **2005,** *152*, A396-A404.

42. Singh, M.; Odusanya, O.; Wilmes, G. M.; Eitouni, H. B.; Gomez, E. D.; Patel, A. J.; Chen, V. L.; Park, J.; Fragouli, P.; Iatrou, H.; Hadjichristidis, N.; Cookson, D.; Balsara, N. P. Effect of Molecular Weight on the Mechanical and Electrical Properties of Block Copolymer Electrolytes. *Macromolecules* **2007,** *40*, 4578-4585.

43. Young, W. S.; Kuan, W. F.; Epps, T. H. Block Copolymer Electrolytes for Rechargeable Lithium Batteries. *J Polym Sci B* **2013,** *52*, 1-16.

44. Weston, J. E.; Steele, B. C. H. Effects of Inert Fillers on the Mechanical and Electrochemical Properties of Lithium Salt-Poly(Ethylene Oxide) Polymer Electrolytes. *Solid State Ion* **1982,** *7*, 75-79.

45. Croce, F.; Appetecchi, G. B.; Persi, L.; Scrosati, B., Nanocomposite Polymer Electrolytes for Lithium Batteries. *Nature* **1998,** *394*, 456-458.

46. Ben Youcef, H.; Garcia-Calvo, O.; Lago, N.; Devaraj, S.; Armand, M., Cross-Linked Solid Polymer Electrolyte for All-Solid-State Rechargeable Lithium Batteries. *Electrochim Acta* **2016,** *220*, 587-594.

47. Khurana, R.; Schaefer, J. L.; Archer, L. A.; Coates, G. W. Suppression of Lithium Dendrite Growth Using Cross-Linked Polyethylene/Poly(ethylene oxide) Electrolytes: A New Approach for Practical Lithium-Metal Polymer Batteries. *J Amer Chem Soc* **2014,** *136*, 7395-7402.

48. Runt, J.; Fitzgerald, J. J. *Dielectric Spectroscopy of Polymeric Materials: Fundamentals and Applications*. American Chemical Society: 1997.

49. Bruce, P. G.; Vincent, C. A. Steady State Current Flow in Solid Binary Electrolyte Cells. *J Electroanal Chem* **1987,** *225*, 1-17.

50. Doyle, M.; Newman, J. Analysis of Transference Number Measurements Based on the Potentiostatic Polarization of Solid Polymer Electrolytes. *J Electrochem Soc* **1995,** *142*, 3465-3468.

51. Chintapalli, M.; Timachova, K.; Olson, K. R.; Mecham, S. J.; Devaux, D.; DeSimone, J. M.; Balsara, N. P. Relationship between Conductivity, Ion Diffusion, and Transference Number in Perfluoropolyether Electrolytes. *Macromolecules* **2016,** *49*, 3508-3515.

52. Newman, J. S.; Thomas-Alyea, K. E. *Electrochemical systems*. J. Wiley: 2004.

53. Gorecki, W.; Jeannin, M.; Belorizky, E.; Roux, C.; Armand, M. Physical Properties of Solid Polymer Electrolyte PEO(LiTFSI) Complexes. *J Phys: Condens Matter* **1995,** *7*, 6823-6832.

54. Timachova, K.; Watanabe, H.; Balsara, N. P. Effect of Molecular Weight and Salt Concentration on Ion Transport and the Transference Number in Polymer Electrolytes. *Macromolecules* **2015,** *48*, 7882-7888.

55. Arumugam, S.; Shi, J.; Tunstall, D. P.; Vincent, C. A. Cation and Anion Diffusion Coefficients in a Solid Polymer Electrolyte Measured by Pulsed-Field-Gradient Nuclear Magnetic Resonance. *J Phys: Condens Matter* **1993,** *5*, 153-160.

56. Sundberg, R. J.; Bruce Martin, R. Interactions of Histidine and Other Imidazole Derivatives with Transition Metal Ions in Chemical and Biological Systems. *Chem Rev* **1974,** *74*, 471-514.

57. Chen, L.; Bos, M.; Grootenhuis, P. D. J.; Christenhusz, A.; Hoogendam, E.; Reinhoudt, D. N.; Van Der Linden, W. E. Stability Constants for Some Divalent Metal Ion/Crown Ether Complexes in Methanol Determined by Polarography and Conductometry. *Anal Chim Acta* **1987,** *201*, 117-125.

58. Appel, M.; Fleischer, G. Investigation of the Chain Length Dependence of Self-Diffusion of Poly(dimethylsiloxane) and Poly(ethylene oxide) in the Melt with Pulsed Field Gradient NMR. *Macromolecules* **1993,** *26*, 5520-5525.

59. Bhattacharja, S.; Smoot, S. W.; Whitmore, D. H. Cation and Anion Diffusion in the Amorphous Phase of the Polymer Electrolyte $(PEO)_8LiCF_3SO_3$. *Solid State Ion* **1986,** *18*, 306-314.

Graphic entry for the Table of Contents (TOC).

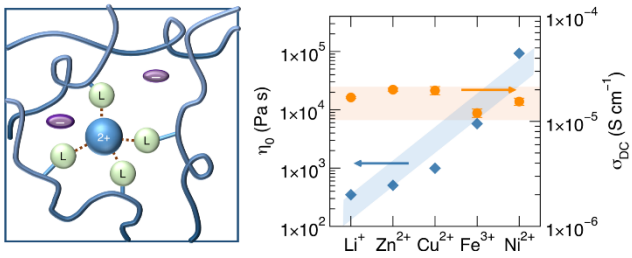

Supporting Information for:

Decoupling Bulk Mechanics and Mono- and Multivalent Ion Transport in Polymers Based on Metal-Ligand Coordination

Nicole S. Schauser,[a, ‡] Gabriel E. Sanoja,[b, ‡] Joshua M. Bartels,[b] Sheetal K. Jain,[c] Jerry Hu,[a] Song-I Han,[c] Lynn M. Walker,[d] Matthew E. Helgeson,[b] Ram Seshadri,[a] Rachel A. Segalman[a,b,]*

[a]Materials Department and Materials Research Laboratory, [b]Department of Chemical Engineering, [c]Department of Chemistry and Biochemistry, University of California, Santa Barbara, California, 93106, United States

[e]Department of Chemical Engineering, Center for Complex Fluids Engineering, Carnegie Mellon University, Pittsburgh, Pennsylvania, 15213, United States

[‡]These authors contributed equally

[*]Email: segalman@ucsb.edu

Molecular Characterization

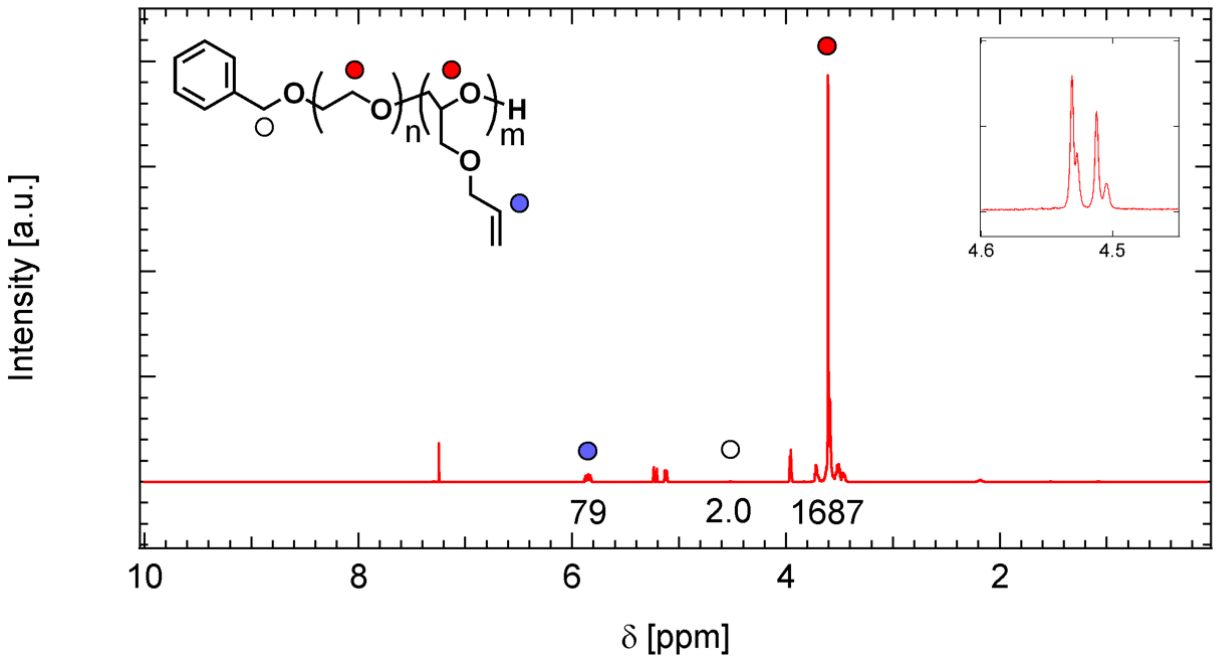

Figure S1: ^{1}H NMR of PEO-*stat*-PAGE in $CDCl_3$. End-group analysis yields the number of repeat units of ethylene oxide and allyl glycidyl ether, PEO_{323}-*stat*-$PAGE_{79}$. Inset illustrates the benzylic hydrogen peaks. This spectrum is collected at a polymer concentration of 60 mg mL^{-1} with 128 scans and a pulse delay time of 5 s.

From the presented ^{1}H NMR, the number of repeat units in PEO-*stat*-PAGE are given by:

$$m = N_{AGE} = \frac{I_{benzylic}}{2} * I_{allylic} = \frac{2.0}{2} * 79 = 79$$

$$n = N_{EO} = \frac{I_{ether} - (5 * N_{AGE})}{4} = \frac{1687 - (5 * 79)}{4} = 323$$

The resulting polymer is then PEO_{323}-*stat*-$PAGE_{79}$. This analysis has been adapted from Lee et al.[1]

Synthesis of Imidazole Functionalized Copolymer (PEO-stat-PIGE)

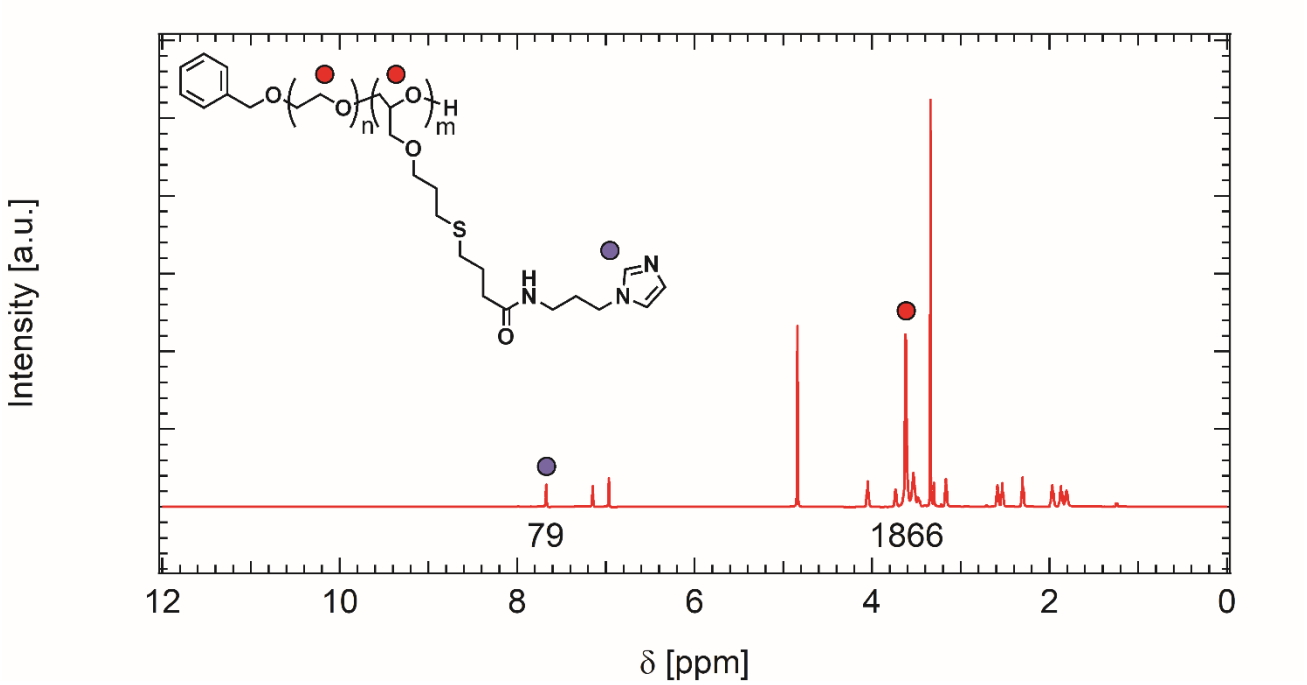

Figure S2: ^{1}H NMR of PEO-*stat*-PIGE in CD_3OD. Disappearance of allyl groups from PEO-*stat*-PAGE and appearance of imidazole aromatic peaks confirm complete conversion during the thiol-ene click reaction.

The presented ^{1}H NMR demonstrates complete conversion of the allylic units into imidazole. The number of repeat units in PEO-*stat*-PIGE are then given by

$$N_{IGE} = \frac{I_{imidazole}}{1} = 79$$

$$N_{EO} = \frac{I_{ether} - (5 * N_{IGE})}{4} = \frac{1866 - (5 * 79)}{4} = 368$$

The resulting polymer is PEO_{368}-*stat*-$PIGE_{79}$, which is consistent with the PEO_{323}-*stat*-$PIGE_{79}$ expected from conservation of moles. For the purposes of this investigation, we use PEO_{323}-*stat*-$PIGE_{79}$ as the ^{1}H NMR end-group analysis requires longer pulse delay times.

Thermal Characterization

Differential scanning calorimetry traces taken upon second heating show a glass transition and absence of a crystallization/melting peak for PEO.

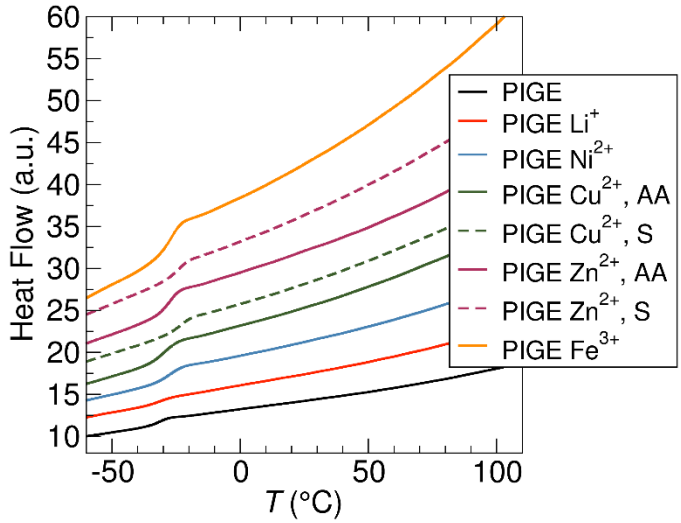

Figure S3. DSC of PIGE mixed with MTFSI salt at an *r* molar ratio of 0.1 show that the T_g does not change significantly with metal identity.

Rheological Characterization

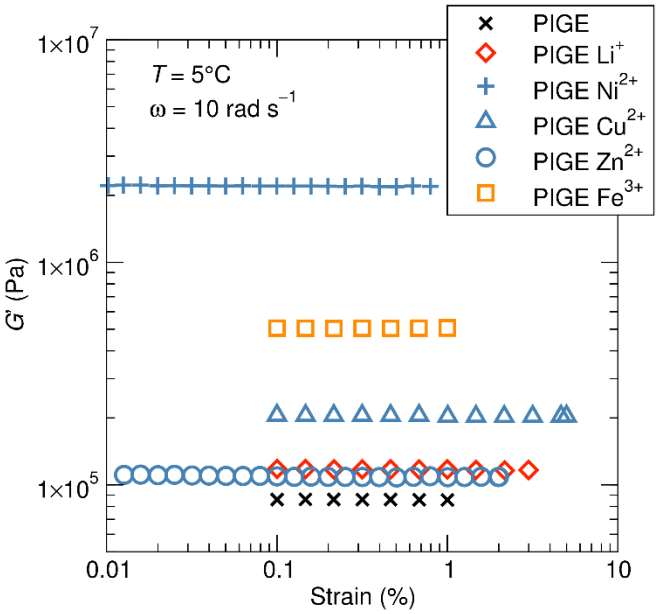

Figure S4: Strain sweeps for polymer samples at *r* = 0.1 performed at 5 °C at a frequency of 10 rad s^{-1}. Each sample's frequency-dependent viscoelastic behavior was measured in the linear regime.

Connection of observed trend in η_0 and M-L dissociation kinetics.

The observed trend in zero-frequency viscosity as a function of metal identity should be described by either the "sticky" Rouse or "sticky" reptation models which suggest the terminal relaxation time scale and zero-frequency viscosity increase as the dissociation rate of the M-L coordination decreases. Dissociation kinetics for Li^+, Ni^{2+}, Cu^{2+}, Zn^{2+} and Fe^{3+} with ligand moieties in aqueous solution have been found to be roughly independent of ligand identity, as the rate-determining step is considered to be the interaction of the M-L complex with water (i.e. a solvent-assisted mechanism).[2-3] It is thus perhaps not surprising that the trend in dissociation kinetics in aqueous solution ($Li^+ \sim Cu^{2+} > Zn^{2+} > Ni^{2+} > Fe^{3+}$) does not correspond to that in zero-frequency viscosity ($Li^+ < Zn^{2+} < Cu^{2+} < Fe^{3+} < Ni^{2+}$) as shown in Figure S5. Data for dissociation kinetics for M-L exchange in bulk polymer melts or even organic solvents is not available for a majority of metal ions and ligands.

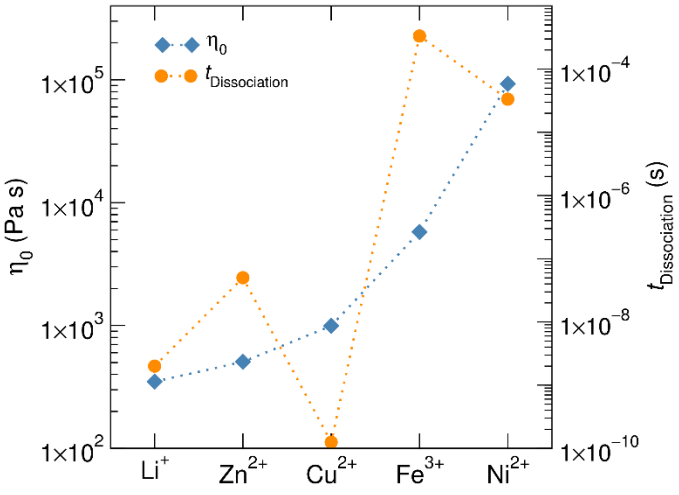

Figure S5. Zero-frequency viscosity trends as a function of cation identity do not follow M-L dissociation kinetics trends ($t_{Dissociation} = \frac{1}{Dissociation\ rate}$) for the given metal ions in aqueous solution.

Ionic Conductivity

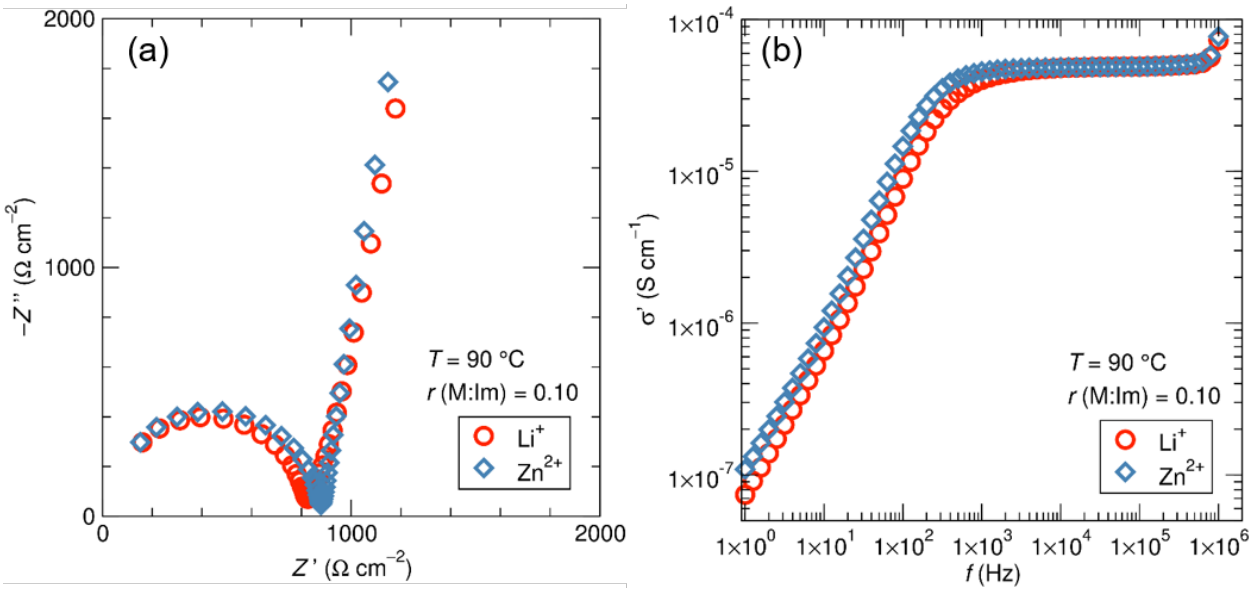

Figure S6: Representative raw conductivity data measured via electrochemical impedance spectroscopy. (a) Raw impedance data for a Li-PIGE and Zn-PIGE sample at 90 °C showing the expected semicircle and diffusion tail. (b) Conductivity representation of the same data, as calculated using the equations presented below.

The impedance data collected was manipulated to calculate the DC ionic conductivity plateau of the data. This was achieved by calculating the real conductivity at the maximum in $\tan(\delta)$[4]

$$c_0 = \frac{\varepsilon_0 Area}{thickness}$$

$$\varepsilon' = \frac{Z''}{\left(Z''^2 + Z'^2\right)\omega c_0}$$

$$\varepsilon'' = \frac{Z'}{\left(Z''^2 + Z'^2\right)\omega c_0}$$

$$\sigma' = \omega \varepsilon'' \varepsilon_0$$

$$\tan(\delta) = \frac{\varepsilon''}{\varepsilon'}$$

$$\sigma_{DC} = \sigma'(\max(\tan(\delta))$$

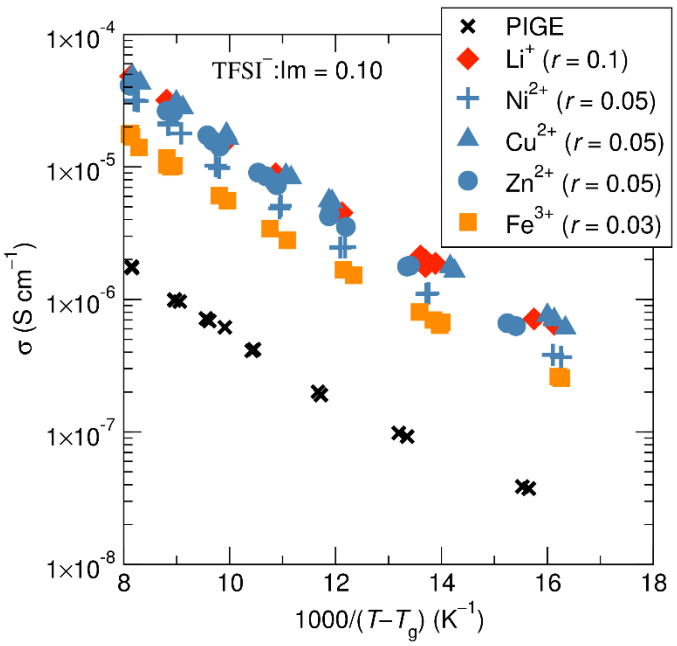

Figure S7: Ionic conductivity values at equal anion:imidazole molar ratios instead of equal metal:imidazole molar ratios. The data does not collapse as well as that normalized by cation, though in general the ionic conductivity seems reasonably impartial to ion identity and concentration.

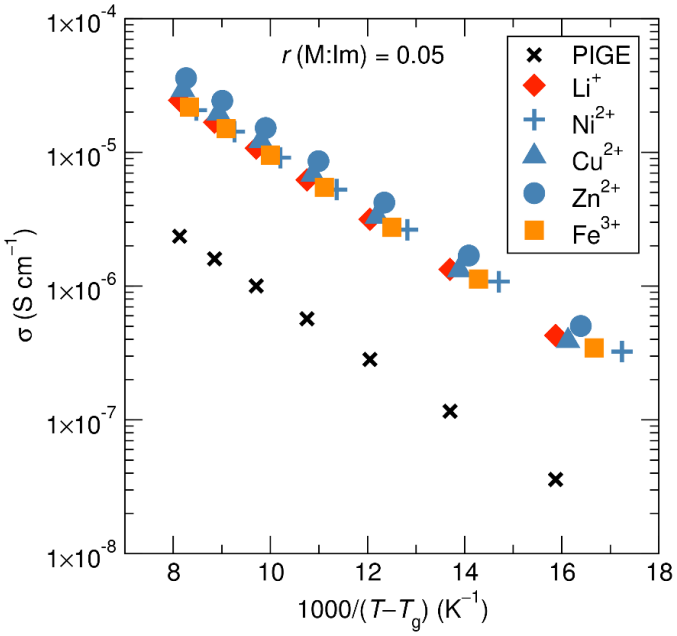

Figure S8: Ionic conductivity as a function of reduced temperature at a molar ratio of metal:imidazole of $r = 0.05$. The data can be approximately normalized by r-ratio.

Table S1. Polymer properties as a function of added metal salt. All polymers are based on the same PIGE precursor, with a degree of polymerization of EO of 323 and of AGE of 79, as determined by ^{1}H NMR. [a] $r = [M^{z+}:\text{Imidaole}]$.

Polymer	r^a	T_g (°C)	σ (μS/cm) at 70 °C	σ (μS/cm) at $T - T_g = 90$ °C
PIGE	0.0	–33	1.0	0.47
PIGE Li^+	0.05	–33	10.7	5.2
PIGE Ni^{2+}	0.05	–28	9.1	5.9
PIGE Cu^{2+}	0.05	–32	12.2	6.0
PIGE Zn^{2+}	0.05	–31	15.2	8.1
PIGE Fe^{3+}	0.05	–30	9.5	5.5

Table S2. Ratios of conductivity between the Li-PIGE and other cation samples are given at three different reduced temperatures adjusted by each sample's glass transition temperature, for $r = 0.05$. Ratios are all very close to 1, suggesting conductivity is approximately governed by the metal-imidazole ratio instead of cation identity or anion concentration.

$T - T_g$	$1000/(T - T_g)$	σ_{Ni}/σ_{Li}	σ_{Zn}/σ_{Li}	σ_{Cu}/σ_{Li}	σ_{Fe}/σ_{Li}
111.11	9	1.04	1.57	1.22	1.01
83.33	12	1.20	1.56	1.14	1.09
66.67	15	1.39	1.55	1.07	1.17

Table S3. Ratios of conductivity between $r = 0.05$ and $r = 0.1$ ($\lambda = \sigma_{r=0.05}/\sigma_{r=0.1}$) are given at three different reduced temperatures adjusted by each sample's glass transition temperature. Ratios are larger than 0.5 (expected for ideal dilute theory with no change in diffusion coefficients), suggesting the diffusion coefficient likely decreases as a function of concentration.

$T - T_g$	$1000/(T - T_g)$	λ_{Li}	λ_{Ni}	λ_{Zn}	λ_{Cu}	λ_{Fe}
111.11	9	0.59	0.60	0.66	0.58	0.71
83.33	12	0.65	0.65	0.62	0.60	0.73
66.67	15	0.73	0.70	0.59	0.61	0.74

PFG NMR

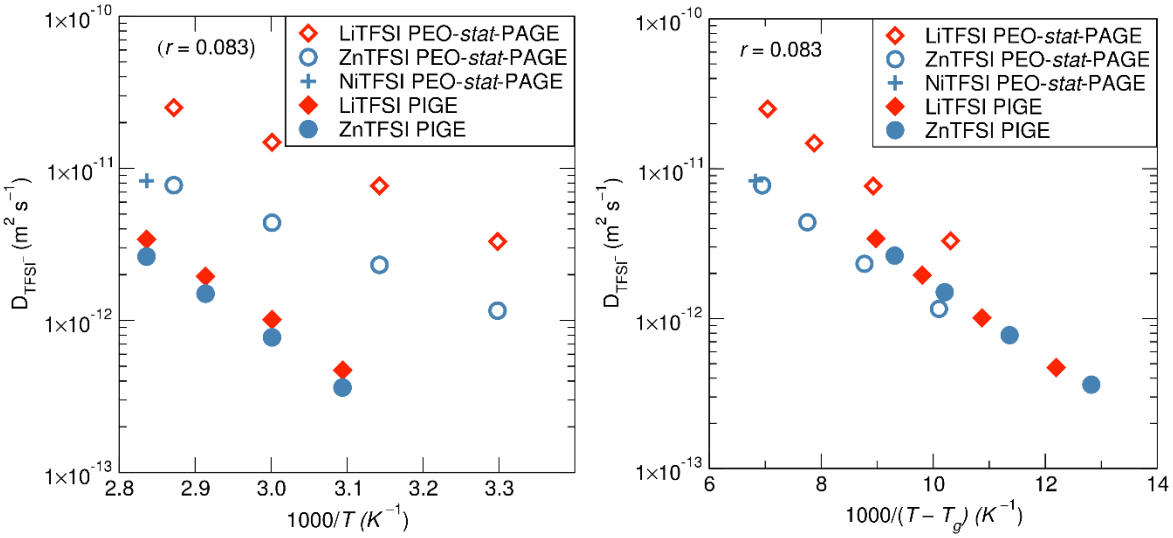

Figure S9: ^{19}F PFG NMR diffusion data as a function of temperature in both PIGE and PEO-*stat*-PAGE polymers. When adjusting for T_g, the $TFSI^-$ diffusion aligns for the Li and Zn PIGE samples, as well as for the Zn and Ni PEO-*stat*-PAGE samples.

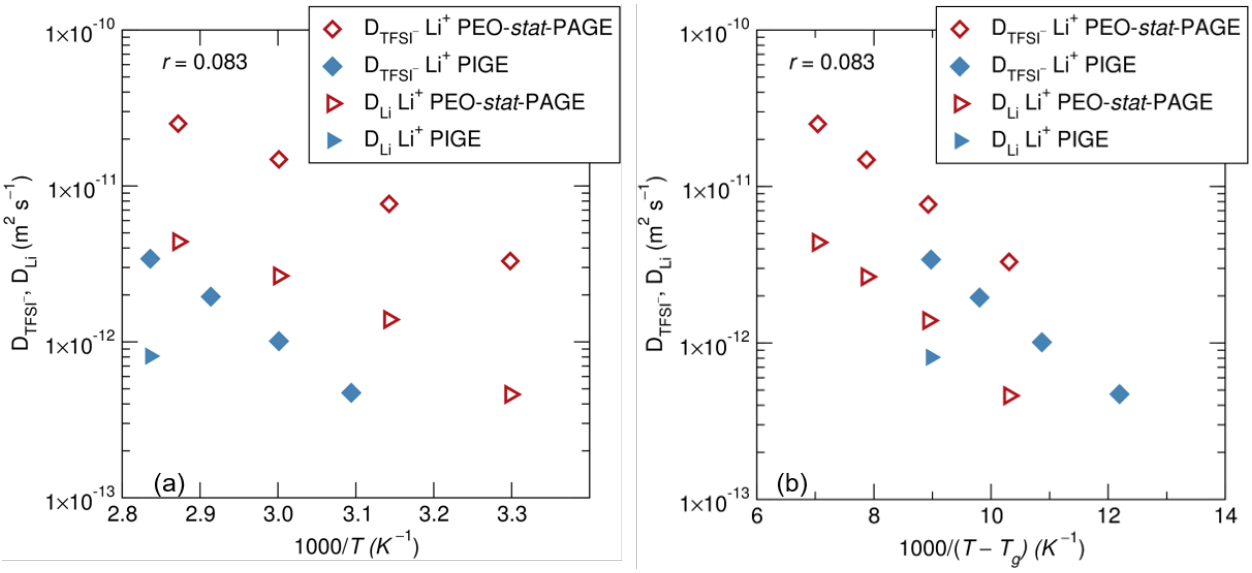

Figure S10: ^{7}Li diffusion (triangles) as measured via PFG NMR is slower than TFSI diffusion (diamonds) for both the PEO-*stat*-PAGE (red open symbols) and PIGE (blue filled symbols) polymers.

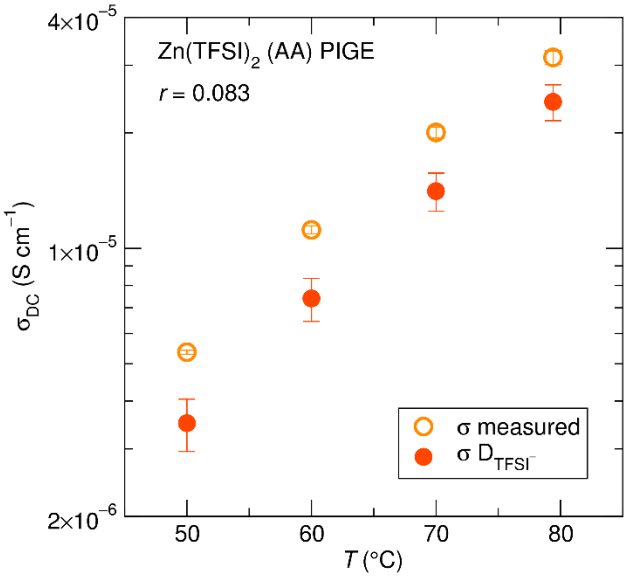

Figure S11: Calculated conductivity compared to impedance spectroscopy measured conductivity for samples prepared with the $Zn(TFSI)_2$ salt sourced from Alfa Aesar show the same trends, though slightly different absolute values, as the $Zn(TFSI)_2$ salt sourced from Solvionic (Figure 6).

Calculation of Zn2+ diffusion coefficient and transference number

From the difference in conductivity measured via impedance spectroscopy (σ_{EIS}) and that calculated from PFG-NMR assuming only $TFSI^-$ mobility (σ_{TFSI-}), one can estimate the contribution to the conductivity from the Zn^{2+} ions. The diffusion coefficient of the Zn^{2+} ions can then be calculated as follows (results in Table S4):

$$\sigma_{TFSI-} = \frac{F^2 c_+}{RT}(z_+ D_-)$$

$$\sigma_{Zn2+} = \sigma_{EIS} - \sigma_{TFSI-}$$

$$D_{Zn2+} = \frac{\sigma_{Zn2+} RT}{F^2 c_+ z_+^2}$$

$$t_+ = \frac{z_+ D_+}{z_+ D_+ + D_-}$$

Table S4. Measured values of EIS conductivity, $TFSI^-$ diffusion coefficient, calculated $TFSI^-$ conductivity, calculated Zn^{2+} conductivity, and calculated Zn^{2+} diffusion coefficient at temperatures between 50 and 80 °C. The cation concentration is estimated as 0.186 mMol cm^{-3} assuming a polymer density of 1.06 g cm^{-3}.

T (°C)	σ_{EIS} (S cm^{-1})	D_{TFSI-} (cm^2 s^{-1})	σ_{TFSI-} (S cm^{-1})	σ_{Zn2+}(S cm^{-1})	D_{Zn2+}(cm^2 s^{-1})	t_+ (Zn^{2+})
50	4.39×10^{-6}	2.33×10^{-9}	3.00×10^{-6}	1.38×10^{-6}	5.36×10^{-10}	0.32
60	9.12×10^{-6}	5.28×10^{-9}	6.60×10^{-6}	2.52×10^{-6}	1.00×10^{-9}	0.28
70	1.62×10^{-5}	1.09×10^{-8}	1.32×10^{-5}	3.01×10^{-6}	1.24×10^{-9}	0.19
80	2.59×10^{-5}	1.91×10^{-8}	2.26×10^{-5}	3.32×10^{-6}	1.40×10^{-9}	0.13

Comparison with PEO-*stat*-PAGE

A similar set of experiments was completed with the PEO-*stat*-PAGE precursor polymer to compare the behavior with the PIGE polymer system. The results show that none of the added metal salts give rise to a viscoelastic response characteristic of a dynamic network, and the conductivity data does not normalize as well even though there are similar inconsequential changes in the glass transition temperatures upon incorporation of salts. This is presumably due to incomplete salt dissociation as suggested by the PFG NMR results on the lithium and zinc PEO-*stat*-PAGE systems; as varying degrees of salt dissociation can greatly affect conductivity due to changes in the concentration of mobile ions. The decreased salt dissociation is attributed to the absence of imidazole pendant groups to enhance dissociation and coordinate the metal cations.

Table S5. PEO-*stat*-PAGE polymer properties as a function of added metal salt. All polymers are based on the same PEO-*stat*-PAGE precursor, with a degree of polymerization of EO of 323 and of AGE of 79, as determined by ^{1}H NMR. [a] $r = [M^{z+}$:AGE]. Only one sample was measured for Zn^{2+} and Fe^{3+}.

Polymer	r^a	T_g (°C)	σ (µS/cm) at 70 °C	σ (µS/cm) at $T - T_g = 90$ °C
PIGE	0.0	–69	0.78 ±0.2	0.083 ±0.02
PIGE Li^+	0.1	–67	170.6 ±18	21.0 ±2
PIGE Ni^{2+}	0.1	–67	159.9 ±30	16.5 ±0.8
PIGE Cu^{2+}	0.1	–67	240.3 ±60	22.2 ±0.6
PIGE Zn^{2+}	0.1	–69	85	9.5
PIGE Fe^{3+}	0.1	–67	95	13.6

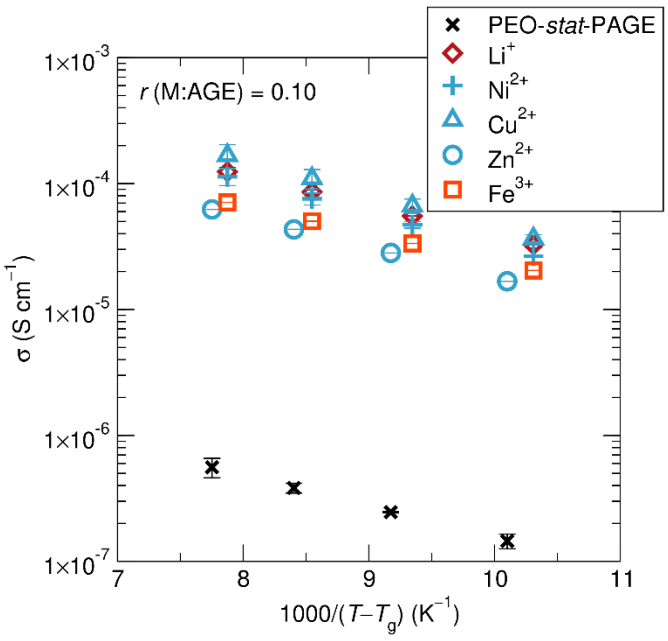

Figure S12: Conductivity measured *via* impedance spectroscopy does not normalize well with molar ratio of metal to AGE groups (*r*). It is possible that the differing interactions with the ether oxygens as compared to the imidazole groups in PIGE account for this discrepancy.

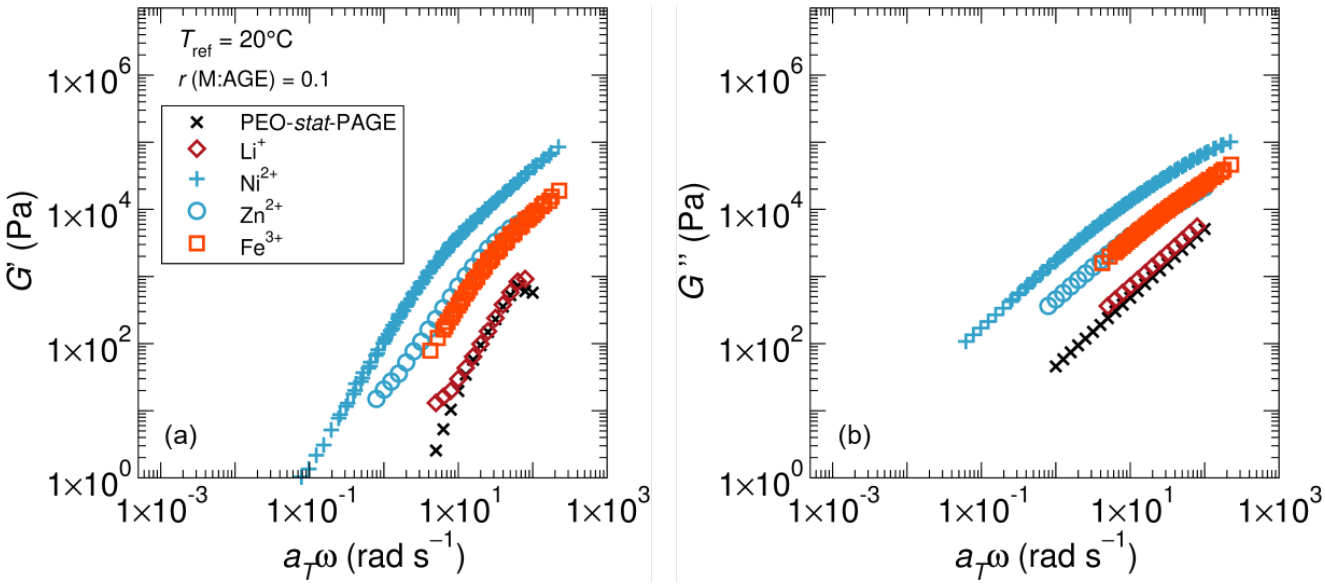

Figure S13: (a) Storage and (b) loss modulus as a function of frequency for the PEO-*stat*-PAGE samples. TTS was performed only on the PEO-*stat*-PAGE Ni^{2+} sample.

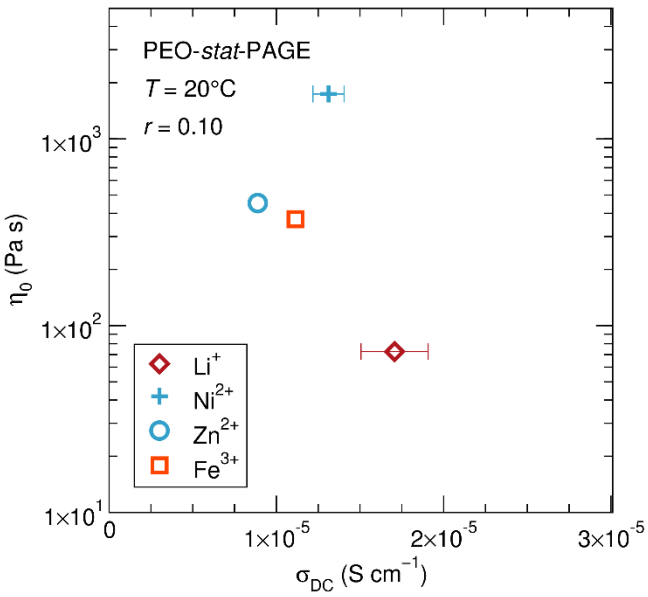

Figure S14. A comparison of the DC ionic conductivity to the zero-shear viscosity shows an improvement from using nickel compared to lithium salts; the improvement is significantly less than that seen in the PIGE system.

$Zn(TFSI)_2$ Purity

The $Zn(TFSI)_2$ salt was tested for purity to confirm that the Zn^{2+} cation is the only other species likely to contribute to ionic conductivity. XRF analysis only detected carbon, fluorine, sulfur and zinc; however the resulting mass percent are not quantitative due to the inability to accurately detect oxygen and nitrogen. Thus, this test was just used to screen for possible impurity elements. Further analysis by ^{19}F solution-state NMR, reveals only one fluorine peak for the $TFSI^-$ anion as expected. Lastly, Karl Fischer titration on the Solvionic salt demonstrated the water content to be at most 0.01 wt% (below the detection limit).

References

1. Lee, B. F.; Wolffs, M.; Delaney, K. T.; Sprafke, J. K.; Leibfarth, F. A.; Hawker, C. J.; Lynd, N. A., Reactivity Ratios and Mechanistic Insight for Anionic Ring-Opening Copolymerization of Epoxides. *Macromolecules* **2012,** *45* (9), 3722-3731.
2. McAuley, A.; Hill, J., Kinetics and Mechanism of Metal-ion Complex Formation in Solution. *Q. Rev. Chem. Soc.* **1962,** *23*, 18-36.

3. Basolo, F.; Pearson, R. G., *Mechanisms of Inorganic Reactions: A Study of Metal Complexes in Solution*. 2 ed.; John Wiley and Sons, Inc.: New York, 1967.
4. Runt, J.; Fitzgerald, J. J., *Dielectric Spectroscopy of Polymeric Materials: Fundamentals and Applications*. American Chemical Society: 1997.